Aerosol Science and Technology

ISSN: (Print) (Online) Journal homepage: www.tandfonline.com/journals/uast20

Effect of viral infection on the ice nucleation efficiency of marine coccolithophores

Alyssa N. Alsante, Daniel C. O. Thornton, Sarah D. Brooks, Jessica A. Mirrielees, Elise K. Wilbourn, Brianna H. Matthews, Ben P. Diaz & Kay D. Bidle

To cite this article: Alyssa N. Alsante, Daniel C. O. Thornton, Sarah D. Brooks, Jessica A. Mirrielees, Elise K. Wilbourn, Brianna H. Matthews, Ben P. Diaz & Kay D. Bidle (22 Nov 2024): Effect of viral infection on the ice nucleation efficiency of marine coccolithophores, Aerosol Science and Technology, DOI: 10.1080/02786826.2024.2420675

To link to this article: https://doi.org/10.1080/02786826.2024.2420675

AEROSOL SCIENCE AND TECHNOLOGY
https://doi.org/10.1080/02786826.2024.2420675

Effect of viral infection on the ice nucleation efficiency of marine coccolithophores

Alyssa N. Alsante[a*], Daniel C. O. Thornton[a], Sarah D. Brooks[b], Jessica A. Mirrielees[b†], Elise K. Wilbourn[b‡], Brianna H. Matthews[b§], Ben P. Diaz[c**], and Kay D. Bidle[c]

[a]Department of Oceanography, Texas A&M University, College Station, Texas, USA; [b]Department of Atmospheric Sciences, Texas A&M University, College Station, Texas, USA; [c]Department of Marine and Coastal Sciences, Rutgers University, New Brunswick, New Jersey, USA

ABSTRACT

A marine coccolithophore (*Emiliania huxleyi*) and coccolithovirus (EhV-207) were grown together in a marine aerosol reference tank (MART) to investigate how the viral lysis of phytoplankton affects the formation of immersion mode ice nucleating particles (INPs) in sea spray aerosol (SSA). The mean ice nucleation temperatures of SSA produced during viral infection were slightly lower (–28.5 °C) than pre-viral infection (–27.5 °C). Ice nucleation temperatures were relatively low, indicating that organic matter from *E. huxleyi* is less effective as an INP than phytoplankton examined in previous studies. *E. huxleyi* is covered in calcium carbonate coccoliths and contains high intracellular concentrations of dimethylsulfoniopropionate (DMSP). The ice nucleation efficiencies of purified components were measured to better understand this model system. Purified coccoliths were moderately effective INPs ($-25.3 \pm 0.4\,^{\circ}C$ at 5×10^{2} mg L^{-1} (mean ± pooled SD)) that showed a concentration effect, with lower freezing temperatures at lower concentrations. Coccoliths and DMSP were both weakly efficient INPs. In comparison, purified phytoplankton viruses (EhV-207 and CtenRNAV-01) infecting coccolithophores and diatoms, respectively, did not affect freezing at temperatures warmer than the procedural blank. Our results suggest that *E. huxleyi*, in contrast to diatoms and cyanobacteria, is not a significant source of immersion mode INPs to the marine atmosphere, despite its broad distribution in the global ocean and large-scale bloom formation.

ARTICLE HISTORY
Received 31 May 2024
Accepted 30 September 2024

EDITOR
Jingkun Jiang

CONTACT Daniel C. O. Thornton dthornton@tamu.edu Department of Oceanography, Texas A&M University, 3146 TAMU Eller O&M Building Room 1204, College Station, TX 77843, USA.
*Current Affiliation: Oak Ridge National Laboratory, Environmental Sciences Division, Oak Ridge, Tennessee, USA.
†Current Affiliation: University of Michigan, Department of Chemistry, Ann Arbor, Michigan, USA.
‡Current Affiliation: Sandia National Laboratories, Bioresource and Environmental Security Department, Livermore, California, USA.
§Current Affiliation: Savannah River National Laboratory, Atmospheric Technologies Group, Aiken, South Carolina, USA.
**Current Affiliation: Sandia National Laboratories, Biotechnology and Bioengineering Department, Livermore, Carolina, USA.
Editor: Jingkun Jiang

Supplemental data for this article can be accessed online at https://doi.org/10.1080/02786826.2024.2420675.

GRAPHICAL ABSTRACT

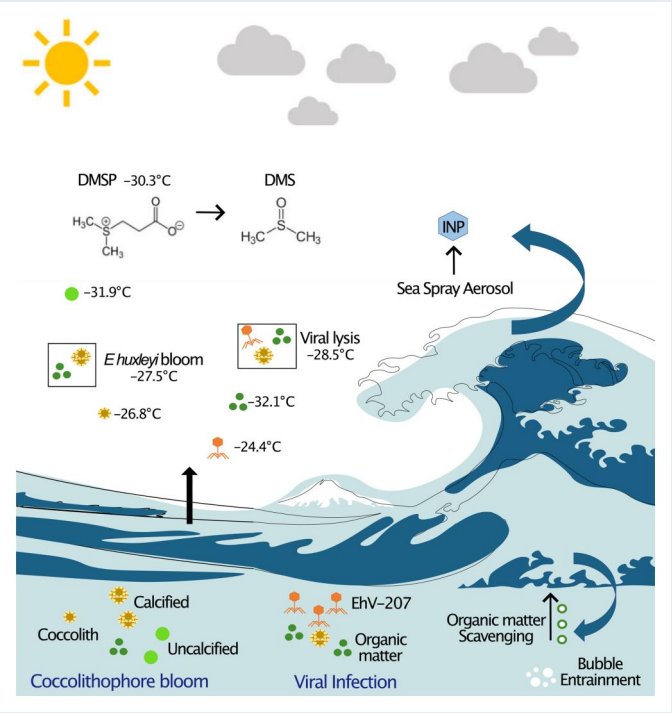

1. Introduction

The effects of aerosol on cloud formation and properties remains one of the largest uncertainties in climate modeling (Boucher et al. 2013). A small subset of aerosol particles (only 1 in every 10^5 aerosol particles, or less) act as ice nucleating particles (INPs), catalyzing the formation of ice-containing clouds at temperatures above the homogeneous freezing temperature of −38 °C in a process known as heterogeneous freezing (Kanji et al. 2017; DeMott et al. 2016; Murray et al. 2012; Rogers et al. 1998). The formation and composition of ice-containing clouds is not well understood, requiring a better understanding of potential sources of aerosol and INPs, particularly from poorly constrained marine sources (Brooks and Thornton 2018; Burrows et al. 2013; Yun and Penner 2013). INPs generated from marine aerosol containing organic matter nucleate ice in both field and laboratory studies (Thornton et al. 2023; Creamean et al. 2019; McCluskey et al. 2017; Wilson et al. 2015; Prather et al. 2013; Alpert, Aller, and Knopf 2011a; Knopf et al. 2011a,b). Several studies have shown phytoplankton produce INPs and that ice nucleation efficiency changes as phytoplankton grow in both experimental systems (Thornton et al. 2023; Mitts et al. 2021; McCluskey et al. 2017; Prather et al. 2013) and in the field (Thornton et al. 2023). Diatoms (Thornton et al. 2023; Wilson et al. 2015; Alpert, Aller, and Knopf 2011a; Knopf et al. 2011), cyanobacteria (Thornton et al. 2023; Wilbourn et al. 2020; Wolf et al. 2019), and chlorophytes (Alpert, Aller, and Knopf 2011b) are all known sources of effective immersion INPs.

In addition to phytoplankton, viruses are enriched in sea spray aerosol (SSA) (Michaud et al. 2018; Rastelli et al. 2017; Sharoni et al. 2015; Lehahn et al. 2014; Aller et al. 2005). The ocean contains an estimated 10^{31} viruses, which are the most abundant biological entities in the ocean (Mojica and Brussaard 2014; Suttle 2007). Viruses are known to play an important role in both regional and global biogeochemical cycling (Mojica and Brussaard 2014; Suttle 2007). Viruses influence phytoplankton bloom termination, with viral lysis resulting in exuded sub-micron sized organic particles and dissolved organic matter (DOM) (Suttle 2007; Wilhelm and Suttle 1999). Studies have shown that a large fraction of biological INPs are sub-micron, placing most marine viruses within the size range of INPs (Irish et al. 2017; McCluskey et al. 2017; Wilson et al. 2015). There are a limited number of studies of non-marine viruses as INPs, with conflicting results (Adams et al. 2021; Cascajo-Castresana et al. 2020; Junge and Swanson

2008). One study determined the tobacco mosaic virus is an efficient INP with initial freezing up to −12 °C (Cascajo-Castresana et al. 2020), whereas another concluded an Arctic freshwater phage is not an efficient INP (Junge and Swanson 2008). The ice nucleation potential of viruses is not well understood, and ice nucleation of phytoplankton viruses has not yet been studied, requiring further investigation as they may play an overlooked role in the formation of marine primary aerosol and INPs.

Emiliania huxleyi is a dominant, globally distributed, bloom-forming coccolithophore species (Taylor, Brownlee, and Wheeler 2017; Paasche 2001). Coccolithophores include calcified strains with a cell wall containing calcium carbonate scales (i.e., coccoliths) and non-calcified strains without coccoliths (Paasche 2001; Green et al. 1998). The calcified strains are dominant, producing blooms covering an area of over 100,000 km^2 annually in the surface ocean (Tyrrell and Merico 2004; Brown and Yoder 1994). Coccoliths from *E. huxleyi* are transferred to the atmosphere in SSA, indicating they may be a source of INPs (Trainic et al. 2018). Multiple large (170–200 nm diameter), double-stranded icosahedral DNA coccolithoviruses infect *E. huxleyi* and are referred to as *E. huxleyi* viruses (EhVs) (Nissimov et al. 2012; Schroeder et al. 2002). EhVs cause the collapse of coccolithophore blooms and are ubiquitous and highly abundant with typical concentrations as high as 10^{10} EhVs L^{-1} in the ocean (Vardi et al. 2012; Schroeder et al. 2003; Bratbak, Egge, and Heldal 1993; Lehahn et al. 2014; Laber et al. 2018). Virus-sized aerosol particles (∼200 nm or less) are potentially transported thousands of kilometers in the atmosphere (Alsante, Thornton, and Brooks 2021). Sharoni et al. (2015) showed that *E. huxleyi* and associated viruses are aerosolized, with potential atmospheric dispersal and infectivity over hundreds of kilometers, indicating their potential for significance in atmospheric processes such as ice nucleation. Cell lysis caused by a viral infection not only releases virus particles into the surrounding water, but also dissolved and particulate organic matter from the lysed phytoplankton cells. This organic matter could potentially be lofted into the atmosphere as SSA.

In this novel study, ice nucleation measurements were conducted on aerosol samples collected above a marine aerosol reference tank (MART) following the growth and lysis of an *E. huxleyi* bloom infected with EhV-207. The overarching goal of the study was to gain a better understanding of the role of virus-phytoplankton interactions on aerosol and INP production from marine sources. In addition, an isolated representative phytoplankton virus (EhV-207) infecting E. *huxleyi* and a ssRNA-containing virus (CtenRNAV-01) (Kranzler et al. 2019; Kranzler et al. 2021; Shirai et al. 2008) infecting the diatom *Chaetoceros tenuissimus* were investigated to understand if and how taxonomically and structurally distinct marine phytoplankton viruses contribute to ice nucleation in the absence of the phytoplankton organic matter released during viral lysis. To the best of our knowledge, this is the first study of marine phytoplankton viruses as INPs and the impact of viral lysis on ice nucleation.

2. Materials and methods

2.1. Marine aerosol reference tank (MART)

2.1.1. MART experimental design

A 227 L acrylic MART containing a culture volume of 63 L was used to provide a controlled environment in which properties of phytoplankton cultures and the aerosol in the headspace above them could be well characterized. Details of the MART tank are provided in our previous work and discussed only briefly here (Figure S1) (Thornton et al. 2023). Initially, *E. huxleyi* (CCMP 374) was grown in batch culture in artificial seawater (ASW) according to Berges, Franklin, and Harrison (2001) amended with 50 µM $NaNO_3$, 5 µM $NaHPO_4$, and full L1 trace metals and vitamins (Guillard and Hargraves 1993). The MART was filled with 63 L of ASW at the same nutrient concentrations as the batch culture. Next, *E. huxleyi* was added to the MART at an initial concentration of $5.0 \times 10^5 \pm 3.0 \times 10^4$ cells L^{-1} and grown over 27 days with the addition of the virus (EhV-207) during late exponential growth (day 10) at a multiplicity of infection (MOI; i.e., number of viruses added per phytoplankton cell) of 16 to initiate a viral lysis event. Two LED light arrays (RAY44, Fluence) were installed on each side of the MART and operated at a photosynthetically active radiation (PAR) of 150 µmol photons m^{-2} s^{-1} in a 14 h on, 10 h off cycle to simulate daylight. The culture was continuously mixed using three 4 cm magnetic stir bars at 180 rpm to keep the cells suspended. The culture temperature was maintained at 16 to 18 °C.

All water samples were collected using a 10% HCl washed 60 mL syringe (VWR) drawn from a 2 cm sample port in the sealed plexiglass lid the tank. Water samples were taken 1.5 to 2 h after the lights turned on. The port was sealed with a silicon rubber bung after the samples were collected.

Before each cycle of aerosol sampling, stirring ceased and the headspace of the MART was flushed with HEPA-filtered air to clear the headspace of background splash-generated aerosol. To generate aerosol *via* a plunging jet, water was pumped from the bottom of the MART to a diffusor located 35.6 cm above the surface water at a rate of 70 L of seawater over approximately 30 min (Watson Marlow 505DZ Peristaltic Pump). The diffusor was rectangular (4 cm), resulting in a laminar waterfall hitting the surface of the water, entraining air as bubbles that rose to the surface and burst, producing aerosol (Fuentes et al. 2010; Sellegri et al. 2006). After a 5 min equilibration period, aerosol were drawn through 1.5 cm PVC tubing *via* a PVC port and passed through a desiccant tube (TSI Inc.) to lower the relative humidity to 50%, which was monitored using a hygrometer (EdgeTech DewPrime II). The aerosol was then passed through a mixing chamber where the sample was split for offline (1 L min^{-1}) and online (1 L min^{-1}) measurements with a mass flow controller (Alicat Scientific). Total particle concentration was monitored using a water-based condensation particle counter (CPC, GRIMM). For offline ice nucleation, aerosol samples were collected from the headspace of the tank for 2 h at a flow rate of 1 L min^{-1} using a PIXE cascade impactor with the L1 stage (0.06 µm − 1 µm) onto pre-combusted (500 °C, 6 h) 25 mm aluminum foil mounted onto polycarbonate disks (PIXE, Inc.). Prior to inoculation with *E. huxleyi*, an aerosol procedural blank from the MART was collected of seawater containing all nutrients to determine the ice nucleation efficiency of aerosol from the seawater in the absence of *E. huxleyi* and *Eh*V-207. The same collection and handling procedures were used for the procedural blank. Aerosol impaction samples were stored at −80 °C until analysis.

2.1.2. Phytoplankton biomass in the MART

Culture (2 mL) was preserved with 2 drops of Lugol's iodine and placed in the dark at 4 °C for no more than two weeks prior to counting (Parsons et al. 1984). Four hundred cells were counted using a hemocytometer (Fuchs-Rosenthal ruling, Hausser Scientific) and a light microscope (Spencer microscope, American Optical) to determine the cell concentration of *E. huxleyi* (CCMP 374) (Guillard and Sieracki 2005).

Chlorophyll *a* concentration was measured according to Arar and Collins (1997). Culture (100 mL) was filtered through 47 mm glass fiber filters (GF/C, Whatman) and placed into 15 mL centrifuge tubes (VWR) at −20 °C until analysis. For extraction, 10 mL of 90% acetone was added to the sample and sonicated (QSonica Q125) for 1 min using 5 s pulses and 5 s between pulses for a total of 2 min on ice to prevent heat buildup. The filters were extracted overnight in 90% acetone at 4 °C in the dark. The extract was centrifuged for 10 min at 4000 × *g*, and the supernatant was decanted and diluted 10-fold. For analysis, 3.5 mL aliquots were placed into quartz glass cuvettes (10 mm, Firefly Scientific) and analyzed using a fluorometer (TD700, Turner Designs) with excitation at 436 nm and emission at 680 nm, giving a concentration of chlorophyll *a* per volume of culture in the MART. Purified chlorophyll *a* from spinach (Sigma Aldrich) was used as a standard for calibration.

2.1.3. Virus-like particle (VLP) enumeration in the MART

The concentration of viruses within the culture was determined using epifluorescence microscopy and SYBR Green I nucleic acid stain (10,000 × concentrate in DMSO, Molecular Probes, ThermoFisher Scientific) (Patel et al. 2007). Culture (0.5 to 2 mL) was fixed with 2% (v/v, final concentration) 0.2 µm-filtered formaldehyde solution and diluted, if necessary, using autoclaved 0.2 µm-filtered artificial seawater (2 mL final sample volume). A GF/F filter (Whatman) was used as a backing for the fragile 0.02 µm Anodisc Al_2O_3 filter (Whatman) and placed onto a sterilized filter tower. The samples were filtered using a vacuum pump at 20 cm Hg vacuum and the filters were stained in a petri dish for 18 min with 100 µl 1:200 (dilution, 5×10^{-3}) SYBR Green I solution diluted with sterile Milli-Q water. Excess dye was removed by blotting the back of the filter using a kimwipe (Kimberly Clark). The stained filter was placed onto a glass microscope slide (VWR) with Diamond SlowFade Antifade (Invitrogen). The slides were stored at −20 °C no longer than one week before enumeration. Four hundred virus particles were counted using an epifluorescent microscope (Zeiss Axioplan 2) with a 100x fluorescence oil-immersion objective.

2.2. Supporting measurements

2.2.1. Purification of marine phytoplankton viruses

The ice nucleation activities of EhV-207 and CtenRNAV-01 were determined from purified virus samples. CtenRNAV-01 is an icosahedral single-stranded RNA (ssRNA) virus 31 nm in diameter infecting the marine diatom, *Chaetoceros tenuissimus* (Shirai et al. 2008). Purified lysates (i.e., viruses

obtained from infection of phytoplankton cultures) were obtained according to Diaz et al. (2023). Briefly, phytoplankton hosts were separately grown in enriched media (F/2 – Si for *E. huxleyi*, SWM-3 for *C. tenuissimus*) to mid-exponential phase in 3 L aerated flasks and infected at a 10:1 virus:host ratio (EhV-207) or a 0.5% (v/v) lysate addition (CtenRNAV-01). Lysates were isolated and purified after *E. huxleyi* was reduced by one to three orders of magnitude from their peak cell concentration. To purify viruses, viral lysates were prefiltered with A/C and G glass fiber filters (Pall Corporation) and concentrated *via* tangential flow filtration (TFF) (10 kDa, Pall Centramate system). Residual salts from media used to grow the phytoplankton hosts (F/2 – Si for *E. huxleyi*, SWM-3 for *C. tenuissimus*) were removed *via* diafiltration with unamended autoclaved coastal New Jersey seawater. Diafiltration from 0.25 L to 1.25 L was repeated four times, harvesting approximately 0.55 L total volume, which was then filtered using a 0.2 μm Sterivex GV filter. Viruses were further purified using six filtered (0.2 μm) cesium chloride ($CsCl_2$) density gradients ranging from 0 to 1.4 g mL^{-1} $CsCl_2$ in 12 mL centrifuge tubes (Beckman Coulter Ultra-Clear, 344059) and ultracentrifuged at 77,000 $\times$ *g* for 4 h at 15 °C (Beckman 80-T Ultracentrifuge, SW 41-T Rotor). The purified viral band was extracted using a sterile serological pipette (VWR) and stored overnight in a total organic carbon (TOC) free vial at 4 °C. The viral concentrate was diafiltered the following day as described above using seawater to reach a total volume of 1.25 L. In addition, a control sample using only autoclaved coastal New Jersey seawater was subjected to the same $CsCl_2$ density gradient purification process. Approximately the same volume of seawater from this control sample with a similar buoyant density to the viruses was sequentially diafiltered against seawater. This control was treated to the same handling procedures and used as a procedural blank for ice nucleation analysis.

EhV-207 was enumerated *via* flow cytometry. For enumeration, the virus sample was fixed with 0.5% glutaraldehyde at 4 °C for 10 min, flash frozen in liquid nitrogen and stored at −20 °C. Frozen and fixed samples were thawed at 35 °C, diluted 1:50 into Tris-EDTA (TE) buffer (pH 7.4) and 1X SYBR Green stained and heated at 80 °C for 10 min (Brussaard 2004). Samples were counted using a BD Biosciences Influx Mariner flow cytometer set to 488 nm excitation and 520 nm emission wavelengths. SYBR Green stained TE buffer was used as a negative control, and sub-micron calibration beads (Spherotech, 0.2 and 0.5 μm) were used to calibrate virus size *via* forward scatter. CtenRNAV-01 was enumerated using the most probable number method (Kranzler et al. 2019). The absence of virus-like particles (VLPs) was confirmed from both samples of the background New Jersey seawater.

Viruses were diluted to within the known concentration range of aerosolized marine viruses in the natural environment (Michaud et al. 2018; Rastelli et al. 2017; Sharoni et al. 2015; Aller et al. 2005). Sharoni et al. (2015) estimated the concentration of aerosolized atmospheric EhVs over the Northeast Atlantic Ocean to be approximately 1×10^7 viruses per L of air based on field observations of seawater concentration and laboratory results of EhV-207 enrichment in aerosol. Both virus (EhV-207 and CtenRNAV-01) samples had an initial concentration of 1×10^9 VLPs L^{-1} and were diluted in ultra-HPLC (uHPLC) water (Sigma Aldrich) to 1×10^7 VLPs L^{-1} to test ice nucleation efficiency at atmospherically relevant concentration.

2.2.2. Uncalcified Emiliania huxleyi and extracellular organic matter

Uncalcified *E. huxleyi* (CCMP 374) was grown in Gulf of Maine seawater (Bigelow NCMA) with full L1 nutrients and harvested during exponential growth at a concentration of $4.5 \times 10^9 \pm 2.3 \times 10^8$ cells L^{-1}. The absence of coccoliths was confirmed at 100x magnification with a light microscope (Spencer microscope, American Optical). Organic matter was harvested from 3 L of uninfected calcified *E. huxleyi* (CCMP 374) grown to $1.4 \times 10^9 \pm 2.0 \times 10^8$ cells L^{-1}. This uninfected exudate culture was prefiltered and concentrated as described above for marine virus samples. The concentrated sample was filtered through 0.2 µm pore-size filter (Sterivex GV) and cooled at 4 °C for 30 min before freezing at −20 °C. The concentration of dissolved organic carbon (DOC) was quantified from three replicates according to Diaz et al. (2023) using a Shimadzu TOC-L Analyzer 680 C Combustion Catalytic Oxidation system with non-dispersive infrared (NDIR) detection and equipped with a combustion tube for high salt samples. Both *E. huxleyi* cells and concentrated dissolved organic matter were diluted 10-fold using uHPLC water to remove NaCl salts with an approximate final concentration of 3.5 g L^{-1} NaCl, the estimated salt concentration of a deliquesced aerosol droplet (Wilbourn et al. 2020). Each 2 µl droplet used for ice nucleation analysis of *E. huxleyi* cells contained approximately 8.9×10^2 cells.

Samples were stored for up to 1 week at −20 °C prior to analysis.

2.2.3. Coccoliths and DMSP concentrations

Coccoliths were extracted from calcified *E. huxleyi* (CCMP 374) according to Jakob et al. (2017). Coccoliths were removed from the phytoplankton cells by heating 950 mL of batch culture at 80 °C for 48 h, resulting in cell disruption with cell fragments and coccoliths settling to the bottom. After cell disruption, 90% of the volume was decanted and discarded, retaining the settled-out coccoliths and cell fragments. The material in the remaining volume was resuspended and divided into 40 mL aliquots into 50 mL sterile polypropylene centrifuge tubes with screw caps (VWR), and centrifuged at 8,000 × *g* for 10 min at 4 °C. The supernatant was removed, and the pellet was resuspended with 3.3 mL of 12.5% (w/v) sodium hypochlorite (NaOCl) and incubated for 15 min at room temperature to remove organic matter *via* oxidation. The extracted coccoliths were cleaned using 5 washes of 6 mM $NaHCO_3$ buffer filled to the 40 mL marking on the centrifuge tube. Between washes, the coccoliths were separated from the wash solution by centrifugation at 1,500 × *g* for 6 min at 4 °C. The pellet containing the coccoliths was retained and the supernatant was discarded. The process was repeated with 5 additional washes of uHPLC water to remove the $NaHCO_3$ buffer. A final concentration of 40 mg L^{-1} purified coccoliths was obtained.

Mixtures of dimethylsulfoniopropionate (DMSP) and coccoliths were used to determine changes in the ice nucleation efficiency of combined inorganic and organic components of *E. huxleyi*, with differences in both chemical composition and physical features. DMSP is an intracellular compound found in very high concentrations (>100 mM) inside *E. huxleyi* cells (Matrai and Keller 1993). DMSP degrades in the water column to form volatile dimethylsulfide (DMS), which oxidizes in the atmosphere through several steps to form non-sea-salt sulfates (Franklin et al. 2010; Bates, Calhoun, and Quinn 1992). It has been debated whether these non-sea-salt sulfate particles are important in cloud condensation nuclei (CCN), facilitating the formation of warm clouds (Quinn and Bates 2011; Charlson et al. 1987). However, the role of DMSP as a potential INP has not been investigated.

We hypothesized that coccoliths or DMSP may suppress ice nucleation in *E. huxleyi*. Isolated coccoliths and DMSP (Sigma Aldrich) were analyzed on their own and in mixtures of DMSP and coccoliths. For the mixtures, the coccolith concentration was 5×10^2 mg L^{-1}, but the concentration of DMSP varied in the mixtures using a 10-fold dilution series in uHPLC water (Sigma Aldrich) from 5×10^4 to 5×10^{-1} mg L^{-1}. Therefore, the mass ratio of coccolith: DMSP ranged from 1:1 to 100,000:1 for the mixtures. Samples were stored for up to one month at −20 °C prior to analysis.

2.3. Ice nucleation measurements

Ice nucleation measurements were performed using either our original custom built ice microscope apparatus (Fornea et al. 2009; Alsante, Thornton, and Brooks 2023; Thornton et al. 2023; Wilbourn et al. 2020; Collier and Brooks 2016) or a slightly modified array apparatus (i.e., a 4 × 4 droplet array to measure up to 16 samples at once), as used in recent studies (Alsante, Thornton, and Brooks 2024; Lei, Chen, and Brooks 2023). The original ice microscope was used for the MART tank aerosol impactor samples collected once per day (Fornea et al. 2009). For the MART samples, 2 µl of uHPLC water was added to the impaction area, immersing the dry aerosol and rinsing them off the hydrophobic aluminum foil impaction stage. A pipettor was used to mix the aerosol into the water and recover the droplet for ice nucleation measurements in the ice microscope. In addition to the MART samples, the ice microscope was used to analyze supporting measurements (see methods) including both coccoliths and DMSP at a concentration of 5×10^2 mg L^{-1}, uncalcified *E. huxleyi*, and exuded organic matter from *E. huxleyi* (Fornea et al. 2009). The sample was placed onto a hydrophobic (coated with Rain-X water repellent, ITW Global Brands) standard glass microscope slide (VWR) and placed inside a sealed cooling stage (Linkam Scientific Instruments, LTS120) mounted onto an optical microscope (Olympus BX43). The temperature of the cooling stage was controlled using a temperature controller (Linkam Scientific Instruments, T96) and a water circulation pump (Linkam Scientific Instruments) using LabSpec 6.2 software (Horiba Instruments, Inc.). The droplet volume was maintained using a constant flow of humidified nitrogen by passing nitrogen gas over a bubbler containing HPLC water (Sigma Aldrich) mixed in a glass mixing chamber. Gas flow rates were controlled using mass flow controllers (Alicat Scientific) and the humidity was monitored using a dew point hygrometer (EdgeTech DewPrime II). The droplet was cooled at a rate of 1 °C min^{-1} from +5 °C to −40 °C. Once the freezing cycle was completed, the droplet warmed to +5 °C where it remained for 1 min to allow complete thawing. The droplet was maintained

between 5 to 25 freezing and thawing cycles, with the mean and standard deviation reported ($n \leq 25$). To determine freezing events, the droplet was monitored using images (Syncerity CCD, Horiba Instruments) recorded every 12 sec with an accuracy of ± 0.2 °C. The ice nucleation temperature was determined from the series of images as the translucent liquid droplet became opaque on freezing. An ice nucleation temperature was not reported if condensation was present on the microscope slide near the droplet or if the droplet changed size due to humidity changes resulting in droplet shrinkage or growth.

The marine virus samples (EhV-207 and CtenRNAV-01), coccolith concentration gradient (10-fold dilution series of 5×10^{1} to 5×10^{-3} mg L^{-1}), and mixtures of coccoliths (5×10^{2} mg L^{-1}) with DMSP (10-fold dilution series of 5×10^{4} to 5×10^{-1} mg L^{-1}) were analyzed to determine the ice nucleation activity using the ice nucleation array due to the larger number of samples (Table S1). To enable the measurement of 16 independent samples simultaneously, a larger glass window (42 mm × 62 mm) was installed in the lid of the Linkam cooling stage of the original ice microscope and a polydimethylsiloxane (PDMS, Sylgard 184, Dow Chemical) spacer was added to hold a sealable 4 × 4 droplet array (Budke and Koop 2015). The microscope was replaced with a high-resolution digital single-lens reflex (DLSR) camera (Canon 5D Mark IV) fitted with a macro lens (Canon EF 100 mm f/2.8). Images were recorded every 6 sec with an accuracy of ±0.3 °C. One droplet was positioned in the center of each well (7 mm diameter) in the array on a Rain-X coated large glass slide with a second glass slide on top of the array to seal the droplets in individual compartments. We note that a humidified flow of nitrogen was not used due to droplet separation into individual compartments by the PDMS spacer. A proposed advantage of the PDMS spacer is that compartmentalization prevents the Wegener-Bergeron-Findeisen (WBF) process, whereby frozen droplets grow in the presence of supercooled liquid droplets due to the vapor pressure difference (Storelvmo and Tan 2015; Murphy and Koop 2005).

PDMS is a widely used hydrophobic and non-porous cross-linked polymeric material (Isenrich et al. 2022; Polen et al. 2018; Budke and Koop 2015). One caveat of the PDMS spacer is that it has poor heat transfer resulting in a temperature gradient across the cooling stage (Polen et al. 2018; Reicher, Segev, and Rudich 2018). Therefore, out of an abundance of caution, the cooling rate was slowed to a rate of 0.5 °C per min to ensure all droplets reached the setpoint temperatures throughout the cooling cycle. A side effect of this was that the +5 °C to −40 °C freeze-thaw cycle could only be performed 12 times (rather than the usual 25 times for the ice microscope). Sixteen droplets can be analyzed at one time resulting in up to 192 freezing data points. For these samples, the pooled mean and standard deviation are reported. As with the ice microscope, a three-point melting point temperature calibration was performed (Fornea et al. 2009). For the array system, an independent calibration was perfomed for each droplet well within the array to compensate for a temperature gradient across the cooling stage.

A 2 µl droplet was used for immersion mode freezing of all samples. A summary of all experiments from each type of sample included in this study and their mean pooled ice nucleation temperatures are shown in Table 1. Additional experimental details including sampling day in the MART time series, concentration or dilution steps (where applicable) and further details on the procedural blanks used for each type of data are included in the online supplementary information (SI; Table S1).

The probability of freezing (P), or fraction of droplets frozen, as a function of temperature (°C) (T) was calculated as (Vali 1971):

$$P(T) = \frac{N_f}{N_0} \quad (1)$$

where N_f is the cumulative number of droplets frozen at a given temperature (T) and N_0 is the total number of freezing events for a sample, compiled from all

Table 1. Overview of biological samples investigated for immersion freezing.

Sample	Replicates	Total number of freezing events	Pooled mean nucleation temperature (°C)
Pre-infection aerosolized MART seawater (Day 0 to 9)	6	125	−27.5 ± 2.0
Post-infection aerosolized MART seawater (Day 11 to 27)	10	240	−28.5 ± 1.4
DMSP	6	138	−30.3 ± 1.3
Coccoliths	55	543	−26.8 ± 1.6
Coccoliths + DMSP	30	360	−25.6 ± 1.0
Uncalcified *E. huxleyi*	5	106	−31.9 ± 0.8
Calcified *E. huxleyi* exuded organic matter	5	125	−32.1 ± 0.8
Virus (EhV-207)	5	55	−24.4 ± 2.1
Virus (CtenRNAV-01)	5	55	−25.3 ± 2.4
Procedural blanks	See Table S1	See Table S1	See Table S1

replicates. This fraction frozen can then be used to calculate the number concentration of INPs (n_{INP}) collected from aerosol in the MART *via* impaction (see Section 2.1.1) using the equation (DeMott et al. 2016):

$$n_{INP}(T) = -\ln\frac{N_u}{N_0} * \frac{V_w}{V_a \times V_s} \quad (2)$$

where N_u is the cumulative number of unfrozen droplets at a given temperature (T) and V_a is the volume of a single aliquot (2 µl for this study). V_w is the total volume of all water droplets (calculated by multiplying V_a by the number of total freezing events) and V_s is the total volume of air sampled on the impactor. The surface-active site density (n) can be calculated from n_{INP} per mass (i.e., coccoliths or DMSP in mg of component) (n_m) or per biological component (i.e., cells, viruses) (n_s) where C_v is the concentration in the sample droplet (Alsante, Thornton, and Brooks 2023; Adams et al. 2021; Vali 1971):

$$n_{m,s}(T) = n_{INP} * \frac{1}{V_a \times C_v} \quad (3)$$

Samples were assigned the following descriptive terms based on their mean immersion freezing temperature: −32 to −25 °C were described as 'weakly effective', −25 to −20 °C as 'moderately effective', −20 to −10 °C were described as 'effective' (Alsante, Thornton, and Brooks 2023; Alsante, Thornton, and Brooks 2024; Matthews, Alsante, and Brooks 2023).

3. Results

3.1. Ice nucleation during viral infection of *Emiliania huxleyi*

To investigate the role of viral infection on ice nucleation in an interactive biological system, the growth and death of a culture of *E. huxleyi* grown in Gulf of Maine seawater was followed for 27 days, with the addition of a coccolithophore virus (EhV-207) during late exponential growth on day 10 to initiate viral infection (Figure 1). Phytoplankton concentration continued to increase after the addition of the virus, peaking on day 12 (Figure 1a). The maximum concentration of *E. huxleyi* was 2.5×10^8 cells L^{-1} with a maximum growth rate on day 7 of 0.95 d^{-1}, as determined by cell concentration (Figure S3). Chlorophyll *a* was also used as an indicator of phytoplankton biomass, with a maximum concentration on day 11 of 16.3 µg chl *a* L^{-1} (Figure 1b). The decline in both chlorophyll *a* (from day 12) and cell concentrations (from day 13) corresponded to an increase in EhV-207 concentration. The maximum concentration of EhV-207 on day 16 was 1.2×10^{10} VLPs L^{-1} (Figure 1c), almost two orders of magnitude larger than the maximum *E. huxleyi* cell concentration.

A list of the immersion mode ice nucleation samples and corresponding freezing temperatures from this study are shown in Table 1 and in the SI (Table S1). The warmest nucleation temperature was observed on day 3 at −25.9 ± 0.6 °C (Figure 1) (mean ± standard deviation), corresponding to the highest growth rate (0.86 d^{-1}; based on cell counts) of samples measured for ice nucleation. The highest fraction frozen was measured on day 3 with only 4% active at −25 °C, but all droplets were active at −27.4 °C, with a maximum number concentration of INPs at 2.2×10^3 INPs L^{-1} air (Figure 2). Day 8 had the second highest nucleation temperature, but there was a large standard deviation (–26.4 ± 4.5 °C) with initial freezing at −17.6 °C and complete freezing at −31.4 °C. An aerosolized seawater procedural blank from the MART had a freezing temperature of −29.0 ± 2.3 °C.

The procedural blank (i.e., aerosolized ASW seawater) was collected and prepared using the same handling procedures as the aerosolized *E. huxleyi* culture (see Section 2.1). The MART samples only contained one independent replicate per day, resulting in a lower statistical robustness for daily freezing temperature data. However, multiple independent replicates were obtained for data from pre-infection ($n = 6$) and post-infection ($n = 10$) of *E. huxleyi*. The remaining supporting measurements of biological components all contain multiple independent replicates ($n \leq 10$). The stability of the freezing temperature from repeated freezing and thawing cycles from MART samples is shown in Figure S2, which indicates that the repeated freeze-thaw cycles did not systematically increase or decrease freezing temperature over time. Number concentrations of INPs were only determined for days in which the median nucleation temperature was warmer than the procedural blank (Figure 2c). Samples with freezing temperatures colder than the procedural blank do not catalyze freezing and therefore do not contain INPs.

A non-parametric one-way analysis of variance (ANOVA) was performed to determine significant differences between daily median ice nucleation temperature using the Kruskal-Wallis test on ranks. Pairwise *post-hoc* comparisons were made with the Wilcoxon test ($p < 0.05$). Days 3 and 8 occurred during the exponential growth phase of the culture and day 3 was the only day significantly different than the aerosolized seawater procedural blank. ($\chi^2 = 140.7$, DF =

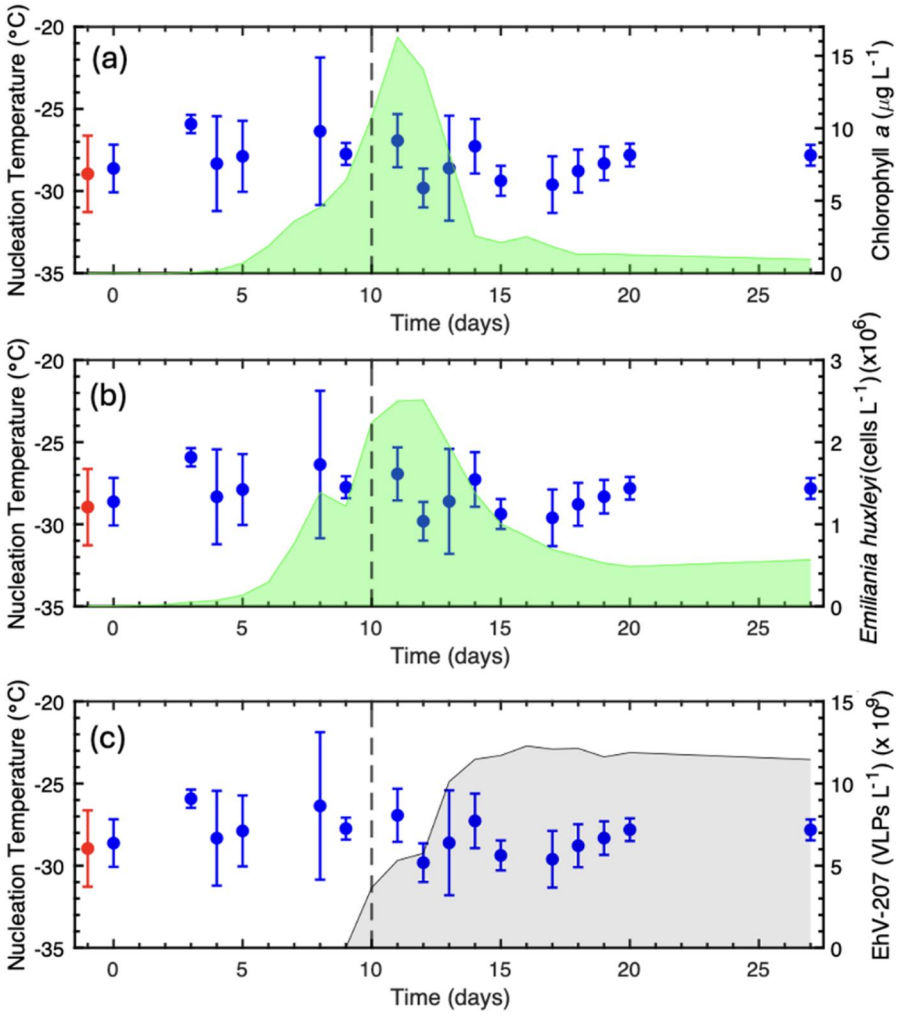

Figure 1. Ice nucleation with changes in *Emiliania huxleyi* biomass and viral concentration over time shown by (a) mean chlorophyll *a* concentration (green shaded region) and (b) mean *E. huxleyi* cell concentration (green shaded region). The viral lysis event is shown after viral infection during late exponential growth on day 10 (dashed black line) with (c) mean EhV-207 concentration (grey shaded region). The daily mean immersion mode nucleation temperatures are shown (solid blue circles) (mean ± standard deviation, $n \geq 15$), and the seawater background blank of aerosol generated from artificial seawater (solid red circle) (mean ± standard deviation, $n = 13$).

16, $p < 0.0001$; Table S2). Daily mean nucleation temperature (i.e., mean from each day freezing temperature was determined) during pre-infection *E. huxleyi* bloom (days 0 to 9) ranged from −25.9 to −28.6 °C and from −26.9 to −29.8 °C during post-infection (days 10 to 27). Overall, the mean nucleation temperature for all days during pre-infection was −27.5 ± 2.0 °C and post-infection was −28.5 ± 1.4 °C (Table 1). The total aerosol concentration in the headspace of the MART did not increase after day 10 (Figure S4), despite the accumulation of *E. huxleyi* biomass during the first 10 days of the culture and the subsequent lysis and fragmentation of the phytoplankton with the introduction of the virus.

The quantum yield of photosystem II (ϕ_{PSII}) was used as an indicator of the physiological status of *E. huxleyi*, with higher values indicating 'healthier' cells able to make a more efficient use of light during photosynthesis (see the SI for methods). During exponential growth in the MART, ϕ_{PSII} increased from a lag-phase low of 0.31 ± 0.02 to a high value of 0.62 ± 0.00 on day 9 (Figure S5). Post infection, ϕ_{PSII} decreased from 0.59 ± 0.01 on day 11 to 0.15 ± 0.02 on day 20 (Figure S5). Viral lysis resulted in lower ice nucleation efficiency when compared to actively growing *E. huxleyi* (Figures 1 and 2). However, *E. huxleyi* was a weakly effective INP throughout the entire growth cycle, including after viral infection. ß-glucosidase enzyme activity (a proxy for bacterial metabolism; Figure S6) and exopolymers (Coomassie staining particles (CSP) and transparent exopolymer particles (TEP); Figure S7) were not related to the ice

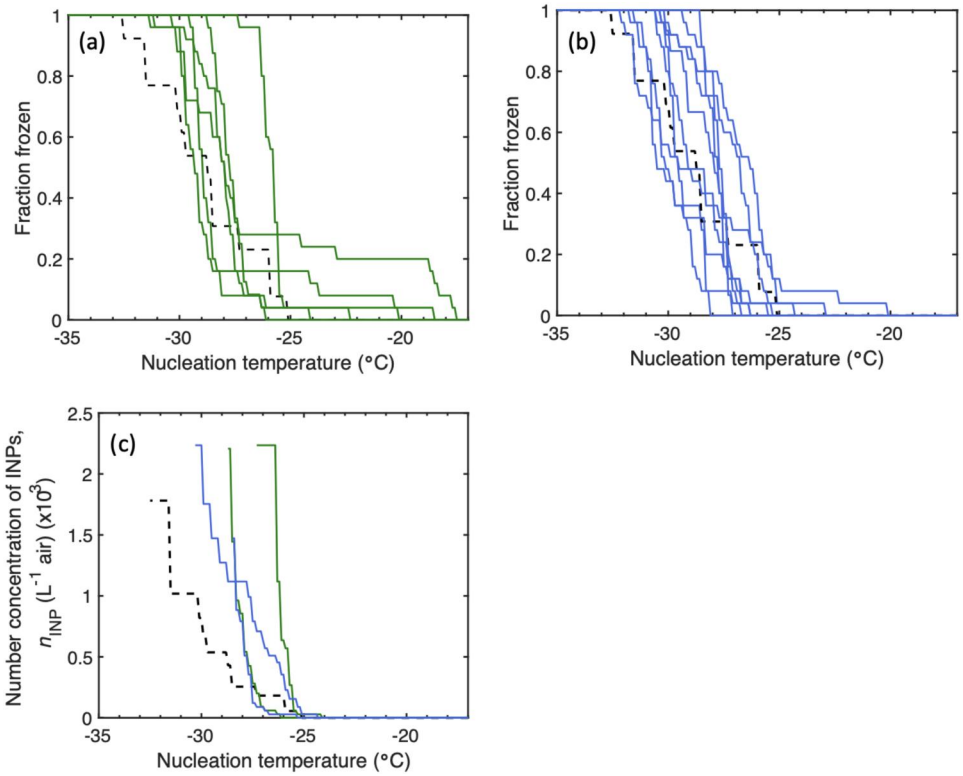

Figure 2. Ice nucleation of *Emiliania huxleyi* with fraction frozen as a function of temperature during (a) pre-infection (solid green lines), (b) post-infection (solid blue lines), and (c) cumulative number concentration of INPs per L of air. The procedural blank is shown for aerosol generated from artificial seawater (black dashed line). Only data that was statistically warmer than the procedural blank was included for the number concentration of INPs.

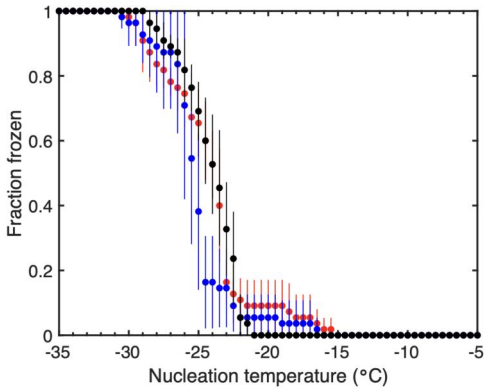

Figure 3. Fraction frozen as a function of temperature of an *Emiliania huxleyi* virus (EhV-207) (blue), a *Chaetoceros tenuissimus* virus (CtenRNAV-01) (red), and the coastal New Jersey seawater procedural blank (black). Data points represent the mean of the pooled data sets ± the 95% confidence limits.

nucleation temperature of the *E. huxleyi* culture (see the SI for methods).

3.2. Ice nucleation of marine phytoplankton viruses

The ice nucleation efficiency of purified marine viruses was determined for purified *E. huxleyi* virus (EhV-207) and a *C. tenuissimus* virus (CtenRNAV-01) isolated from phytoplankton cultures in coastal New Jersey seawater (Table 1). Both EhV-207 (−24.4 ± 2.1 °C) and CtenRNAV-01 (−25.3 ± 2.4 °C) were moderately efficient INPs. More than 65% of EhV-207 INPs were active at −25 °C and only 38% of CtenRNAV-01 INPs active at the same temperature (Figure 3). Although both marine viruses had similar mean freezing temperatures, they were significantly different due to the observed variability in freezing temperature ($\chi^2 = 11.0$, DF = 2, $p < 0.0042$). However, neither virus improved ice nucleation efficiency when compared to the background coastal New Jersey seawater procedural blank subject to the same purification procedures (−24.5 ± 1.5 °C) and therefore the cumulative number of active sites (n_s) was not determined (Table S1). Only CtenRNAV-01 was statistically different than the procedural blank, resulting in depression of the nucleation temperature ($\chi^2 = 11.0$, DF = 2, $p < 0.0042$).

3.3. Ice nucleation of inorganic and organic components of Emiliania huxleyi

To better understand how the chemical composition of *E. huxleyi* influenced its ice nucleation efficiency,

we investigated specific inorganic and organic components isolated from *E. huxleyi*. Exuded organic matter from *E. huxleyi* with 6.80 ± 0.11 mg DOC L^{-1} had a mean nucleation temperature of $-32.1 \pm 0.8\,^{\circ}C$ and depressed the nucleation temperature of the coastal New Jersey seawater procedural blank the original culture was grown in ($-29.2 \pm 0.4\,^{\circ}C$) (Table S1). Less than 2% of INPs from the *E. huxleyi* organic matter were active at $-25\,^{\circ}C$ and were not completely active until $-35\,^{\circ}C$ (Figure 4a), with a n_s of less than $1 \times 10^{\circ}$ per mg of DOC at this temperature (Figure 4b).

It was previously hypothesized that calcium carbonate from coccoliths is responsible for the inefficient immersion mode ice nucleation efficiency of *E. huxleyi* (Ladino et al. 2016; Alpert, Aller, and Knopf 2011b). However, only the ice nucleation efficiency of mineral calcite has been investigated and was determined to be ice nucleation inactive (Kaufmann et al. 2016). Isolated and purified coccoliths from calcifying *E. huxleyi* was measured at a concentration of 5×10^2 mg of coccoliths L^{-1}, representative of the concentration used to determine the ice nucleation efficiencies of other biological compounds (Alsante, Thornton, and Brooks 2023). Coccoliths were moderately effective INPs with a mean nucleation temperature of $-25.3 \pm 0.4\,^{\circ}C$ (Table S1). Over 30% of INPs were activated at $-25\,^{\circ}C$ with a n_s of 3.7×10^2 per mg of coccoliths at this temperature (Figure 4b). The effect of coccoliths on ice nucleation was also determined by comparing the ice nucleation of calcifying *E. huxleyi* with an uncalcified strain that does not produce coccoliths. The mean nucleation temperature of uncalcified *E. huxleyi* was $-31.9 \pm 0.8\,^{\circ}C$, and the mean nucleation temperature of the procedural blank (Gulf of Maine seawater used to grow the culture) was $-32.7 \pm 1.4\,^{\circ}C$ (Table S1). Uncalcified *E. huxleyi* was a weakly effective INP with no INPs active at $-25\,^{\circ}C$, and approximately 10% of INPs active at $-30\,^{\circ}C$ (Figure 4). The cumulative number of active sites was not determined for uncalcified *E. huxleyi* because it was not statistically warmer than the procedural blank.

DMSP was a weakly effective INP with a mean nucleation temperature of $-30.3 \pm 1.3\,^{\circ}C$ (Table S1). Less than 2% of INPs were active at $-25\,^{\circ}C$ and by $30\,^{\circ}C$, only 50% of INPs were active with a corresponding n_s of 6.5×10^1 per mg of DMSP (Figure 4).

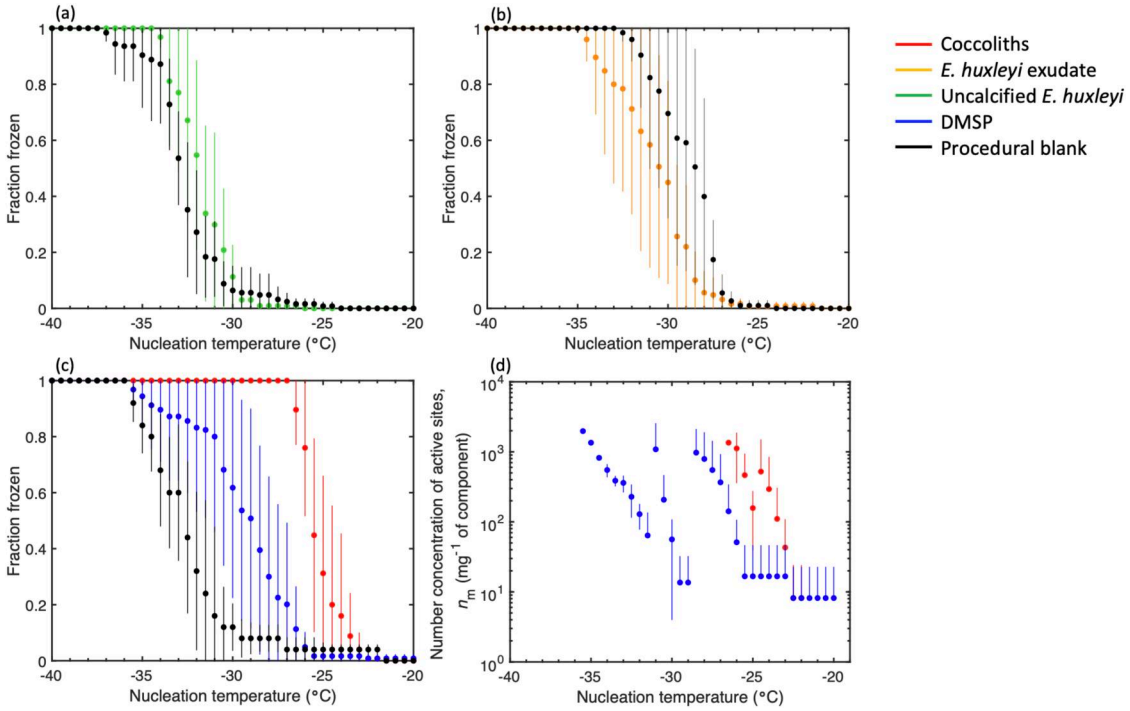

Figure 4. Ice nucleation of components of *Emiliania huxleyi* with (a–c) fraction frozen as a function of temperature and (d) number concentration of ice nucleation active sites per mg of coccolith (red), per mg of carbon from *Emiliania huxleyi* exudate (orange), per mg of dimethylsulfoniopropionate (blue), and per cell from uncalcified *E. huxleyi* (green). Background coastal New Jersey seawater is shown for *E. huxleyi* exudate (black) and Gulf of Maine seawater for uncalcified *E. huxleyi* (black) used to grow the phytoplankton. A procedural blank (uHPLC water) is shown for the samples of purified coccoliths and DMSP (black). Data points represent the mean of the pooled data sets ± the 95% confidence limits. Only data that was statistically warmer than the corresponding procedural blank was included for the number concentration of ice nucleation active sites.

3.4. Effect of concentration on the ice nucleation of coccoliths and mixtures of coccoliths with DMSP

To better understand the role of coccoliths on ice nucleation, the ice nucleation efficiency of coccoliths was investigated over a range of concentrations (5×10^{1} to 5×10^{-3} mg L^{-1}) using the ice nucleation array apparatus (Table 1). These measurements were in addition to the concentration of 5×10^{2} mg L^{-1}, which was measured using the ice microscope. The lowest concentration of 5×10^{-3} mg coccoliths L^{-1} was representative of the mass concentration of coccoliths found in the open ocean during an *E. huxleyi* bloom (Linge Johnsen and Bollmann 2020). Figure 5 only contains the cumulative number of active sites for concentrations that were statistically warmer than the procedural blank. The warmest mean nucleation temperature was observed at high concentration (-25.2 ± 1.4 °C at 5×10^{1} mg L^{-1}) and was moderately efficient with almost 40% of INPs active and a n_s of 4.7×10^{3} ice nucleation active sites per mg of coccoliths at −25 °C (Figure 5). There was no statistical difference between the two different custom-built ice nucleation apparatuses at the two highest concentrations of purified coccoliths (5×10^{2} mg L^{-1} for the single droplet system and 5×10^{1} mg L^{-1} for the array system; Table S1). The three higher concentrations investigated (5×10^{1} to 5×10^{-2} mg L^{-1}) were all statistically different than the background uHPLC water procedural blank ($\chi^2 = 163.1$, DF = 11, $p < 0.0001$). The lowest concentrations investigated (5×10^{-2} and 5×10^{-3} mg L^{-1}) were only weakly effective INPs (mean freezing temperatures of -28.1 ± 1.5 and -27.9 ± 2.3 °C, respectively) and not statistically different than the background uHPLC water procedural blank ($\chi^2 = 163.1$, DF = 11, $p < 0.0001$).

We also investigated the role of purified coccolith and DMSP mixtures at a constant concentration of 5×10^{2} mg coccoliths L^{-1} with a range of DMSP concentrations (5×10^{4} to 5×10^{-1} mg L^{-1}). The mean freezing temperature of the mixture of coccoliths with 5×10^{2} mg DMSP L^{-1} was -25.3 ± 0.8 °C with 40% frozen at −25 °C (Figure 5c), which was not statistically different from purified coccoliths at the same concentration in the absence of DMSP with over 30% of INPs frozen −25 °C (χ^2 = 163.1, DF = 11,

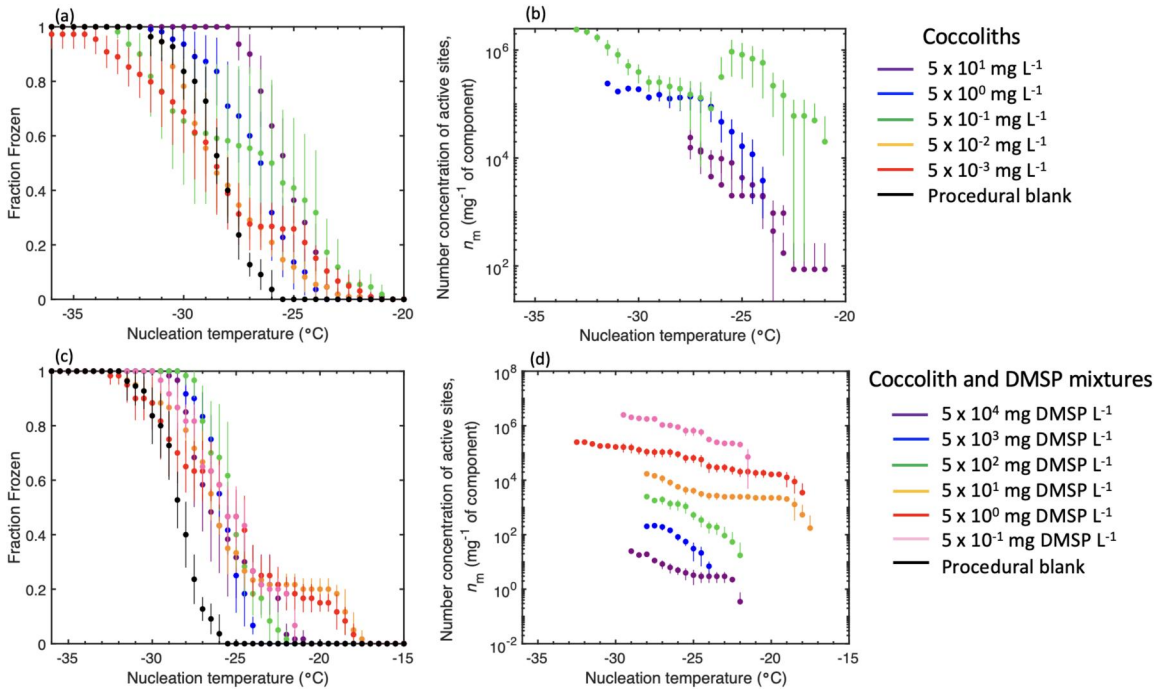

Figure 5. Ice nucleation of purified coccolith concentration gradient with (a) fraction frozen as a function of temperature and (b) number of ice nucleation active sites per mg of coccoliths at 5×10^{1} mg L^{-1} (purple), 5×10^{0} mg L^{-1} (blue), 5×10^{-1} mg L^{-1} (green), 5×10^{-2} mg L^{-1} (orange), and 5×10^{-3} mg L^{-1} (red). Ice nucleation of coccolith (5×10^{2} mg L^{-1}) mixtures with varying dimethylsulfoniopropionate (DMSP) concentration of the (c) fraction frozen as a function of temperature and (d) active site density per mg of DMSP at 5×10^{4} mg L^{-1} (purple), 5×10^{3} mg L^{-1} (blue), 5×10^{2} mg L^{-1} (green), 5×10^{1} mg L^{-1} (orange), 5×10^{0} mg L^{-1} (red), and 5×10^{-1} mg L^{-1} (pink). A procedural blank (uHPLC water) was used to dilute purified coccoliths (black). Data points represent the mean of the pooled data sets ± the 95% confidence limits. Only data that was statistically warmer than the corresponding procedural blank was included for the number concentration of ice nucleation active sites.

$p < 0.0001$). Mixtures of coccoliths at lower concentrations of DMSP ranging from 5×10^1 mg L^{-1} to 5×10^0 mg L^{-1} had similar mean freezing temperatures (–25.2 to −25.4 °C; Table S1) but were statistically different due to the observed larger variation in freezing temperature when compared to purified coccoliths at these concentrations ($\chi^2 = 163.1$, DF = 11, $p < 0.0001$). Mixtures of DMSP with purified coccoliths had the highest number concentration of ice nucleation active sites at high DMSP concentrations with a maximum n_s of approximately 10^6 per mg at −25 °C (Figure 5d).

3.5. Comparison of E. huxleyi and biological components

Figure 6 illustrates differences in the median freezing temperature of all of the biological INPs from this study (Table 1). A non-parametric one-way analysis of variance (ANOVA) was performed to determine significant differences between median ice nucleation temperature using the Kruskal-Wallis test on ranks for the MART results (i.e., pre-infection and post-infection) and supporting measurements (i.e., uncalcified *E. huxleyi*, *E. huxleyi* organic and inorganic components, and the two marine viruses across all investigated concentrations). Pairwise *post-hoc* comparisons were made

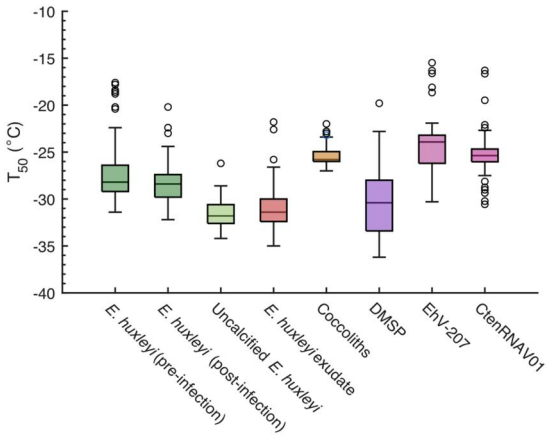

Figure 6. Median nucleation temperatures (T_{50}) for biological ice nucleating particles (INPs) from this study of *Emiliania huxleyi* grown in the marine aerosol reference tank (MART) on days of pre-infection (day 0 to 10) and post-infection (day 11 to 27) (dark green), uncalcified *E. huxleyi* (light green), exuded matter from calcified *E. huxleyi* (red), purified coccoliths at 5×10^{-4} mg L^{-1} (brown), dimethylsulfoniopropionate (DMSP) at 5×10^{-4} mg L^{-1} (blue), and marine viruses infecting *E. huxleyi* (EhV-207) and *Chaetoceros tenuissimus* (CtenRNAV-01) (pink). Median nucleation temperature (T_{50}) is shown by the black horizontal lines within each box. Black boxes represent the first and third quartile. The black vertical lines connected to each box plot represents the range with outliers indicated by black circles.

with the Wilcoxon test ($p < 0.05$) ($\chi^2 = 576.0$, DF = 7, $p < 0.0001$; Table S3). The ice nucleation temperature during the pre-infection *E. huxleyi* bloom was significantly warmer than post-infection. In addition, both the organic matter (i.e., exudate) and DMSP released from *E. huxleyi* had a significantly lower ice nucleation efficiency than *E. huxleyi* grown in the MART and purified EhV-207. In contrast, coccoliths froze at significantly warmer temperatures than both calcified and uncalcified *E. huxleyi* with combined nucleation temperatures from all investigated concentrations.

4. Discussion

Viruses have been proposed to be important INPs (Rahlff et al. 2023; McCluskey et al. 2017; Wilson et al. 2015) and some purified viruses improve ice nucleation efficiency in the immersion mode (Rahlff et al. 2023; Adams et al. 2021; Cascajo-Castresana et al. 2020). We showed two contrasting marine phytoplankton viruses are moderately efficient INPs but did not improve ice nucleation when compared to the seawater procedural blank, both of which were diluted using uHPLC water to remove salts. Viral lysis of *E. huxleyi* with EhV-207 led to the release of both organic matter and inorganic coccoliths, resulting in lower ice nucleation efficiency when compared to both actively growing *E. huxleyi* and purified EhV-207. These results suggest *E. huxleyi* may be depressing the freezing temperature of EhV-207 viruses during viral lysis.

Our ice nucleation measurements encompassed the pre- and post-viral infection time periods of *E. huxleyi* culture in the MART, with 6 samples taken pre-infection and 10 samples post-infection. This enabled us to test the hypothesis that viral infection enhances the production of INPs, and a comparison of the ice nucleation temperatures pre- and post-infection indicated that viral infection did not change the effectiveness of aerosol to act as INPs. Changes occurred in the culture over the 28 days of sampling, in addition to the addition of the virus on day 10, such as shifts in the physiological status of the phytoplankton driven by the depletion of nutrients. These changes may have interacted with the effects of the viral infection. However, it is difficult to uncouple these interactions, as the viral infection itself affected changes, such as a decrease in growth rate (Figure S3).

The collection of replicate samples for ice nucleation from the tank on a single day was not logistically possible. Aerosol collection in the MART occurred over 2 h, sampling 120 L from the 164 L headspace.

Therefore, each sample represents a population of aerosol collected on that day. The samples were exposed to repeated freeze-thaw cycles, which have been shown to change the nucleation temperature of biogenic immersion ice nuclei from *Pseudomonas syringae* (Eufemio et al. 2023) and surfactant mixtures (Perkins et al. 2020). This was not observed in our experiment (Figure S2), where there was no decreasing or increasing trend in nucleation temperature over an excess of 20 freeze-thaw cycles in samples collected from the MART. Other biological INPs also show no effect of being exposed to repeated freeze-thaw cycles, including INP from lichens (Eufemio et al. 2023) and the protein ribulose-1,5-bisphosphate carboxylase/oxygenase (RuBisCO) (Alsante, Thornton, and Brooks 2024).

Phytoplankton have been shown to be ice nucleation active at warm freezing temperatures (Thornton et al. 2023; Ickes et al. 2020; Wilbourn et al. 2020; Wilson et al. 2015; Knopf et al. 2011). Therefore, we investigated individual inorganic and organic components of *E. huxleyi* to determine why *E. huxleyi* was a source of relatively inefficient INP. The coccosphere, the cell covering made from calcium carbonate scales (coccoliths), is a key difference between coccolithophores (including *E. huxleyi*) and other groups of phytoplankton. Alpert, Aller, and Knopf (2011b) measured immersion mode ice nucleation by *E. huxleyi* and found that it did not act as an INP, which they hypothesized was due to coccoliths. Manson (1957) determined that the mineral calcite is not an INP in the immersion mode. Calcite is the form of calcium carbonate found in coccoliths (Lee 2008), suggesting that coccoliths may explain why *E. huxleyi* was a relatively inefficient INP, and the presence of coccoliths may be responsible for depressing the ice nucleation of more efficient INP in the cells, such as proteins and nucleic acids (Alsante, Thornton, and Brooks 2023). However, we demonstrated that coccoliths were not responsible for the low ice nucleation efficiency of *E. huxleyi*; purified coccoliths in the absence of *E. huxleyi* cells were moderately efficient INPs at high concentration (5×10^2 and 5×10^1 mg of coccoliths L^{-1}). Further support for this conclusion comes from the observation that the ice nucleation efficiency of a naked strain of *E. huxleyi*, which did not produce coccoliths, was lower than that of the strain with coccoliths.

Infection of *E. huxleyi* with EhV has shown to increase aerosolized coccolith concentration by up to an order of magnitude (Trainic et al. 2018). However, the ice nucleation temperature of aerosol collected from the MART tank decreased after viral infection, indicating that the coccoliths, or any other lysis product of *E. huxleyi*, did not increase ice nucleation efficiency during viral lysis. We did not measure the concentration of coccoliths or other cell components in the aerosol before and after lysis, therefore we do not know how lysis changed the composition of the aerosol.

Concentration affects the ice nucleation efficiency of some organic species, such as protein and lignin, with higher ice nucleation efficiency associated with aggregation at relatively high concentrations (Alsante, Thornton, and Brooks 2024; Bogler and Borduas-Dedekind 2020; Cascajo-Castresana et al. 2020; Eickhoff et al. 2019). The ice nucleation efficiency of a concentration gradient of purified inorganic coccoliths was investigated. The two highest concentrations were moderately efficient (5×10^2 and 5×10^1 mg coccoliths L^{-1}), but at lower concentrations (5×10^0 to 5×10^{-3} mg coccoliths L^{-1}), the freezing temperature decreased. Concentrations consistent with the mass of coccoliths found in the North Atlantic were only weakly effective INPs (5×10^{-2} mg coccoliths L^{-1}). Organic matter associated with the coccoliths was removed by oxidation, and light microscopy showed that the coccoliths were not aggregated. Warmer ice nucleation temperatures at high concentration may be due to an increased number of defects including grooves and cracks that act to form hydrophobic and hydrophilic areas when compared to a smooth surface (Pruppacher and Klett 1997). Water molecules may favorably bind to a disordered cluster of water molecules within defects, facilitating ice crystal formation. Coccoliths were shown to have a low natural aerosolization of only one coccolith per 1×10^8 coccoliths in seawater during an *E. huxleyi* bloom (Trainic et al. 2018). Therefore, based on the results of both coccolith aerosolization and ice nucleation, it is unlikely that coccoliths are a significant source of INPs over the ocean.

Previous work has shown that fast-growing phytoplankton produce organic matter containing the most efficient INPs (Thornton et al. 2023), a result that agrees with our finding that the most effective INPs in the MART were associated with the exponential growth of *E. huxleyi* before the addition of the virus. However, only one day of *E. huxleyi* exponential growth had a significantly different ice nucleation efficiency than the aerosolized MART seawater background, and there was a large variability in freezing temperature. Thornton et al. (2023) investigated the ice nucleation efficiency of two different

phytoplankton species in the MART, a cyanobacterium (*Synechococcus elongatus*) and a diatom (*Thalassiosira weissflogii*). Both species resulted in the production of efficient INPs, with mean ice nucleation temperatures as high as −15 °C during exponential growth (Figure S8). *E. huxleyi* had a lower fraction of INPs frozen than both *S. elongatus* and *T. weissflogii* during exponential growth in the MART. The difference between *E. huxleyi* and other species of phytoplankton indicate that there may be chemical differences between taxa that affect ice nucleation (Ickes et al. 2020; Wilbourn et al. 2020; Wilson et al. 2015; Thornton et al. 2023). This contrasts with our comparison of *S. elongatus* and *T. weissflogii*, which suggested that fast growing phytoplankton with a relatively high quantum yield of photosystem II, produced aerosol that were the most efficient immersion mode INPs. Based on these observations, Thornton et al. (2023) suggested that physiological status is a predictor of efficient INPs from marine phytoplankton and more useful than biomass or phylogeny. However, the results from this experiment indicate that both physiological status and phylogeny are important.

In addition to the low ice nucleation efficiency of *E. huxleyi* cells, a previous study found that exuded organic matter from *E. huxleyi* was not an effective INP in the deposition mode (Ladino et al. 2016). However, exuded organic matter from other phytoplankton species has been shown to increase ice nucleation efficiency (McCluskey et al. 2017; Wilson et al. 2015; Knopf et al. 2011). Ladino et al. (2016) did not investigate the chemical composition of organic matter resulting in the poor ice nucleation of this organism. Several potential molecular candidates could negatively affect the ice nucleation of coccolithophores. It is well known that coccolithophores have a distinct carbon metabolism from other phytoplankton groups, with carbon stored predominately in low molecular weight compounds such as mannitol (Obata et al. 2013). In addition, coccolithophores possess distinct acidic polysaccharides and alkenones (Taylor, Brownlee, and Wheeler 2017; Tsuji et al. 2015). *E. huxleyi* accumulates high concentrations (up to 400 mM) of DMSP within the cell (Taylor, Brownlee, and Wheeler 2017), which differentiates it from many other taxa that do not contain intracellular DMSP or contain it at much lower concentrations, such as diatoms (Keller 1988). Some studies have used atmospheric concentrations of DMS, which is derived from DMSP, to track marine airmasses originating from locations of high biological activity (Porter et al. 2022; Sanchez et al. 2018; Mukai, Yokouchi, and Suzuki 1995). This is because some marine phytoplankton produce large amounts of DMSP, and the resulting DMS has a short short atmospheric lifetime (Porter et al. 2022; Sanchez et al. 2018; Mukai, Yokouchi, and Suzuki 1995). Porter et al. (2022) found no correlation between DMS and INP concentration in the Arctic atmosphere.

We demonstrated that DMSP is a weakly effective INP, and therefore both laboratory and field measurements indicate it is highly unlikely to contribute to atmospheric ice nucleation. We hypothesized that DMSP was depressing the freezing temperature in aerosol from *E. huxleyi*. However, there was no evidence of DMSP depressing the freezing temperature of purified coccoliths when ice nucleation efficiency was measured in mixtures of the two components. Differences in the composition of organic matter in *E. huxleyi* cells may be responsible for the relatively low ice nucleation efficiency compared with the other phytoplankton taxa that have been measured as immersion INPs (Thornton et al. 2023; Wilbourn et al. 2020; Alpert, Aller, and Knopf 2011b; Knopf et al. 2011). We showed that the presence of organic matter from *E. huxleyi* resulted in a loss of moderate ice nucleation efficiency of both coccoliths and EhV-207.

5. Conclusions

This study was designed to test the potential effect of the viral lysis of phytoplankton on the generation of immersion mode ice nucleating particles (INPs) in sea spray aerosol (SSA). The mean ice nucleation temperatures of SSA produced during viral infection were slightly lower (–28.5 °C) than pre-viral infection (–27.5 °C). Ice nucleation temperatures were relatively cold, indicating that organic matter from *E. huxleyi* is less effective as an INP than phytoplankton examined in previous studies. This low ice nucleation efficiency of *E. huxleyi* compared with other phytoplankton, and the depression in the freezing temperature of EhV-207 during viral lysis led us to investigate the ice nucleation efficiency of individual components of this coccolithophore species. High concentrations of coccoliths were moderately efficient INPs. However, in concentrations more representative of the open ocean, coccolithophores were only weakly efficient, agreeing with nucleation temperatures during an *E. huxleyi* bloom in the MART. Our results suggest that composition or morphology differences between coccolithophores and other phytoplankton groups, such as diatoms and cyanobacteria, are responsible for coccolithophores' low ice nucleation efficiency.

In addition, the three phytoplankton groups (diatoms, cyanobacteria, and coccolithophores) we investigated in the MART (this study and Thornton et al. 2023) have different geographic distributions. Given that their ice nucleation efficiencies vary as well, this may be an indication that biological aerosol have different ice nucleation efficiencies at different latitudes. Modeling studies of organic aerosol and INP concentrations show distinct geographic differences over marine regions (Zhao et al. 2021). For example, the Irish Sea is known to produce vast blooms of coccolithophores annually, but modeling indicates low contributions of marine organics to the total INP fraction in this region. Our results suggest parameterizations should consider the ice nucleation efficiency of individual groups of phytoplankton to predict ice nucleation efficiency more accurately from remote marine regions. More research is needed to understand taxonomic differences in ice nucleation efficiency and what causes these differences, which will lead to a better understanding of biological INPs from remote marine regions and their properties.

Disclosure statement

No potential conflict of interest was reported by the author(s).

Funding

This work was supported by the National Science Foundation (NSF) from the Division of Atmospheric and Geospace Scences (AGS) [USA; grant numbers AGS-1539881 and AGS-2128133].

ORCID

Alyssa N. Alsante http://orcid.org/0000-0001-6905-4769
Daniel C. O. Thornton http://orcid.org/0000-0001-5546-5161
Sarah D. Brooks http://orcid.org/0000-0001-8185-9332
Jessica A. Mirrielees http://orcid.org/0000-0003-2678-3720
Elise K. Wilbourn http://orcid.org/0000-0002-2599-9864
Brianna H. Matthews http://orcid.org/0000-0002-3905-2049
Kay D. Bidle http://orcid.org/0000-0003-4170-412X

References

Adams, M. P., N. S. Atanasova, S. Sofieva, J. Ravantti, A. Heikkinen, Z. Brasseur, J. Duplissy, D. H. Bamford, and B. J. Murray. 2021. Ice nucleation by viruses and their potential for cloud glaciation. *Biogeosciences* 18 (14): 4431–44. doi:10.5194/bg-18-4431-2021.

Aller, J. Y., M. R. Kuznetsova, C. J. Jahns, and P. F. Kemp. 2005. The sea surface microlayer as a source of viral and bacterial enrichment in marine aerosols. *J. Aerosol Sci.* 36 (5-6):801–12. doi:10.1016/j.jaerosci.2004.10.012.

Alpert, P. A., J. Y. Aller, and D. A. Knopf. 2011a. Ice nucleation from aqueous NaCl droplets with and without marine diatoms. *Atmos. Chem. Phys.* 11 (12):5539–55. doi:10.5194/acp-11-5539-2011.

Alpert, P. A., J. Y. Aller, and D. A. Knopf. 2011b. Initiation of the ice phase by marine biogenic surfaces in supersaturated gas and supercooled aqueous phases. *J. Phys. Chem. A* 13 (44):19882–94. doi:10.1039/c1cp21844a.

Alsante, A. N., D. C. O. Thornton, and S. D. Brooks. 2024. Effect of aggregation and molecular size on the ice nucleation efficiency of proteins. *Environ. Sci. Technol.* 58 (10): 4594–605. doi:10.1021/acs.est.3c06835.

Alsante, A. N., D. C. O. Thornton, and S. D. Brooks. 2023. Ice nucleation catalyzed by the photosynthesis enzyme RuBisCO and other abundant biomolecules. *Commun. Earth Environ.* 4 (1):51. doi:10.1038/s43247-023-00707-7.

Alsante, A. N., D. C. O. Thornton, and S. D. Brooks. 2021. Ocean Aerobiology. *Front. Microbiol.* 12:764178. doi:10.3389/fmicb.2021.764178.

Arar, E. J., and G. B. Collins. 1997. *Method 445.0 – In vitro determination of chlorophyll a and pheophytin a in marine and freshwater algae by fluorescence*. Cincinnati: United States Environmental Protection Agency, Office of Research and Development, National Exposure Research Laboratory.

Bates, T. S., J. A. Calhoun, and P. K. Quinn. 1992. Variations in the methanesulfonate to sulfate molar ratio in submicrometer marine aerosol particles over the South Pacific Ocean. *J. Geophys. Res.* 97 (D9):9859–65. doi:10.1029/92JD00411.

Berges, J. A., D. J. Franklin, and P. J. Harrison. 2001. Evolution of an artificial seawater medium: Improvements in enriched seawater, artificial water over the last two decades. *J. Phycol.* 37 (6):1138–45. doi:10.1046/j.1529-8817.2001.01052.x.

Bogler, S., and N. Borduas-Dedekind. 2020. Lignin's ability to nucleate ice via immersion freezing and its stability towards physicochemical treatments and atmospheric processing. *Atmos. Chem. Phys.* 20 (23):14509–22. doi:10.5194/acp-20-14509-2020.

Boucher, O., D. Randall, P. Artaxo, C. Bretherton, G. Feingold, P. Forster, V. M. Kerminen, Y. Kondo, H. Liao, U. Lohmann, et al. 2013. Clouds and aerosols. Climate Change 2013 the Physical Science Basis: Working Group I Contribution to the Fifth Assessment Report of the Intergovernmental Panel on Climate Change 571–658.

Bratbak, G., J. K. Egge, and M. Heldal. 1993. Viral mortality of the marine alga. *Emiliania huxleyi* (Haptophyceae) and termination of algal blooms. *Mar. Ecol. Prog. Ser.* 93:39–48. doi:10.3354/meps093039.

Brooks, S. D., and D. C. O. Thornton. 2018. Marine Aerosols and Clouds. *Annu. Rev. Mar. Sci.* 10 (1):289–313. doi:10.1146/annurev-marine-121916-063148.

Brown, C. W., and J. A. Yoder. 1994. Coccolithophorid blooms in the global ocean. *J. Geophys. Res.* 99 (C4): 7467–82. doi:10.1029/93JC02156.

Brussaard, C. P. D. 2004. Optimization of Procedures for Counting Viruses by Flow Cytometry. *Appl. Environ. Microbiol.* 70 (3):1506–13. doi:10.1128/AEM.70.3.1506-1513.2004.

Budke, C., and T. Koop. 2015. BINARY: An optical freezing array for assessing temperature and time dependence of heterogeneous ice nucleation. *Atmos. Meas. Tech.* 8 (2): 689–703. doi:10.5194/amt-8-689-2015.

Burrows, S. M., C. Hoose, U. Pöschl, and M. G. Lawrence. 2013. Ice nuclei in marine air: Biogenic particles or dust? *Atmos. Chem. Phys.* 13 (1):245–67. doi:10.5194/acp-13-245-2013.

Cascajo-Castresana, M., R. O. David, M. A. Iriarte-Alonso, A. M. Bittner, and C. Marcolli. 2020. Protein aggregates nucleate ice: The example of apoferritin. *Atmos. Chem. Phys.* 20 (6):3291–315. doi:10.5194/acp-20-3291-2020.

Charlson, R. J., J. E. Lovelock, M. O. Andreae, and S. G. Warren. 1987. 6114. Oceanic phytoplankton, atmospheric sulphur, cloud albedo and climate. *Nature.* 326 (6114): 655–61. doi:10.1038/326655a0.

Collier, K. N., and S. D. Brooks. 2016. Role of Organic Hydrocarbons in Atmospheric Ice Formation via Contact Freezing. *J. Phys. Chem. A.* 120 (51):10169–80. doi:10.1021/acs.jpca.6b11890.

Creamean, J. M., J. N. Cross, R. Pickart, L. McRaven, P. Lin, A. Pacini, R. Hanlon, D. G. Schmale, J. Ceniceros, T. Aydell, et al. 2019. Ice Nucleating Particles Carried From Below a Phytoplankton Bloom to the Arctic Atmosphere. *Geophys. Res. Lett.* 46 (14):8572–81. doi:10.1029/2019GL083039.

DeMott, P. J., T. C. J. Hill, C. S. McCluskey, K. A. Prather, D. B. Collins, R. C. Sullivan, M. J. Ruppel, R. H. Mason, V. E. Irish, T. Lee, et al. 2016. Sea spray aerosol as a unique source of ice nucleating particles. *Proc. Natl. Acad. Sci. USA* 113 (21):5797–803. doi:10.1073/pnas.1514034112.

Diaz, B. P., F. Gallo, R. H. Moore, and K. D. Bidle. 2023. Virus infection of phytoplankton increases average molar mass and reduces hygroscopicity of aerosolized organic matter. *Sci. Rep.* 13 (1):7361. doi:10.1038/s41598-023-33818-4.

Eickhoff, L., K. Dreischmeier, A. Zipori, V. Sirotinskaya, C. Adar, N. Reicher, I. Braslavsky, Y. Rudich, and T. Koop. 2019. Contrasting Behavior of Antifreeze Proteins: Ice Growth Inhibitors and Ice Nucleation Promoters. *J. Phys. Chem. Lett.* 10 (5):966–72. doi:10.1021/acs.jpclett.8b03719.

Eufemio, R. J., I. de Almeida Ribeiro, T. L. Sformo, G. A. Laursen, V. Molinero, J. Fröhlich-Nowoisky, M. Bonn, and K. Meister. 2023. Lichen species across Alaska produce highly active and stable ice nucleators. *Biogeosciences* 20 (13):2805–12. doi:10.5194/bg-20-2805-2023.

Fornea, A. P., S. D. Brooks, J. B. Dooley, and A. Saha. 2009. Heterogeneous freezing of ice on atmospheric aerosols containing ash, soot, and soil. *J. Geophys. Res.* 114 (D13): 58. doi:10.1029/2009JD011958.

Franklin, D. J., M. Steinke, J. Young, I. Probert, and G. Malin. 2010. Dimethylsulphoniopropionate (DMSP), DMSP-lyase activity (DLA) and dimethylsulphide (DMS) in 10 species of coccolithophore. *Mar. Ecol. Prog. Ser.* 410:13–23. doi:10.3354/meps08596.

Fuentes, E., H. Coe, D. Green, G. de Leeuw, and G. Mcfiggans. 2010. Laboratory-generated primary marine aerosol via bubble-bursting and atomization. *Atmos. Meas. Tech.* 3 (1):141–62. doi:10.5194/amt-3-141-2010.

Green, J. C., B. R. Heimdal, E. Paasche, and R. Moate. 1998. Changes in calcification and the dimensions of coccoliths of Emiliania huxleyi (Haptophyta) grown at reduced salinities. *Phycologia* 37 (2):121–31. doi:10.2216/i0031-8884-37-2-121.1.

Guillard, R., and M. Sieracki. 2005. Counting cells in cultures with the light Microscope. In *Algal culturing techniques*, ed. R. A. Andersen, 239–252. Burlington, MA: Elsevier Academic Press.

Guillard, R. R. L., and P. E. Hargraves. 1993. *Stichochrysis immobilis* is a diatom, not a chrysophyte. *Phycologia* 32 (3):234–6. doi:10.2216/i0031-8884-32-3-234.1.

Hoppe, H.-G. 1983. Significance of exoenzymatic activities in the ecology of brackish water: Measurements by means of methylumbelliferyl-substrates. *Marine Ecol. Prog. Series* 11:299–308. doi:10.3354/meps011299.

Ickes, L., G. C. E. Porter, R. Wagner, M. P. Adams, S. Bierbauer, A. K. Bertram, M. Bilde, S. Christiansen, A. M. L. Ekman, E. Gorokhova, et al. 2020. The ice-nucleating activity of Arctic sea surface microlayer samples and marine algal cultures. *Atmos. Chem. Phys.* 20 (18):11089–117. doi:10.5194/acp-20-11089-2020.

Irish, V. E., P. Elizondo, J. Chen, C. Chou, J. Charette, M. Lizotte, L. A. Ladino, T. W. Wilson, M. Gosselin, B. J. Murray, et al. 2017. Ice-nucleating particles in Canadian Arctic sea-surface microlayer and bulk seawater. *Atmos. Chem. Phys.* 17 (17):10583–95. doi:10.5194/acp-17-10583-2017.

Isenrich, F. N., N. Shardt, M. Rösch, J. Nette, S. Stavrakis, C. Marcolli, Z. A. Kanji, A. J. deMello, and U. Lohmann. 2022. The Microfluidic Ice Nuclei Counter Zürich (MINCZ): a platform for homogeneous and heterogeneous ice nucleation. *Atmos. Meas. Tech.* 15 (18):5367–81. doi:10.5194/amt-15-5367-2022.

Jakob, I., M. A. Chairopoulou, M. Vučak, C. Posten, and U. Teipel. 2017. Biogenic calcite particles from microalgae – Coccoliths as a potential raw material. *Eng. Life Sci.* 17 (6):605–12. doi:10.1002/elsc.201600183.

Junge, K., and B. D. Swanson. 2008. High-resolution ice nucleation spectra of sea-ice bacteria: Implications for cloud formation and life in frozen environments. *Biogeosciences* 5 (3):865–73. doi:10.5194/bg-5-865-2008.

Kanji, Z. A., L. A. Ladino, H. Wex, Y. Boose, M. Burkert-Kohn, D. J. Cziczo, and M. Krämer. 2017. Overview of Ice Nucleating Particles. *Meteorological Monographs* 58: 1.1–.33. doi:10.1175/AMSMONOGRAPHS-D-16-0006.1.

Kaufmann, L., C. Marcolli, J. Hofer, V. Pinti, C. R. Hoyle, and T. Peter. 2016. Ice nucleation efficiency of natural dust samples in the immersion mode. *Atmos. Chem. Phys.* 16 (17):11177–206. doi:10.5194/acp-16-11177-2016.

Keller, M. D. 1988. Biological Oceanography Dimethyl Sulfide Production and Marine Phytoplankton: The Importance of Species Composition and Cell Size Dimethyl Sulfide Production and Marine Phytoplankton: The Importance of Species Composition and Cell Size. *Biological Oceanography* 6:375–82. doi:10.1080/01965581.1988.10749540.

Knopf, D. A., P. A. Alpert, B. Wang, and J. Y. Aller. 2011. Stimulation of ice nucleation by marine diatoms. *Nature Geosci.* 4 (2):88–90. doi:10.1038/ngeo1037.

Kranzler, C. F., J. W. Krause, M. A. Brzezinski, B. R. Edwards, W. P. Biggs, M. Maniscalco, J. P. McCrow, B. A. S. van Mooy, K. D. Bidle, A. E. Allen, et al. 2019. Silicon limitation facilitates virus infection and mortality

of marine diatoms. *Nat. Microbiol.* 4 (11):1790–7. doi:10.1038/s41564-019-0502-x.

Kranzler, C. F., M. A. Brzezinski, N. R. Cohen, R. H. Lampe, M. Maniscalco, C. P. Till, J. Mack, J. R. Latham, K. W. Bruland, B. S. Twining, et al. 2021. Impaired viral infection and reduced mortality of diatoms in iron-limited oceanic regions. *Nat. Geosci.* 14 (4):231–7. doi:10.1038/s41561-021-00711-6.

Laber, C. P., J. E. Hunter, F. Carvalho, J. R. Collins, E. J. Hunter, B. M. Schieler, E. Boss, K. More, M. Frada, K. Thamatrakoln, et al. 2018. Coccolithovirus facilitation of carbon export in the North Atlantic. *Nat. Microbiol.* 3 (5):537–47. doi:10.1038/s41564-018-0128-4.

Ladino, L. A., J. D. Yakobi-Hancock, W. P. Kilthau, R. H. Mason, M. Si, J. Li, L. A. Miller, C. L. Schiller, J. A. Huffman, J. Y. Aller, et al. 2016. Addressing the ice nucleating abilities of marine aerosol: A combination of deposition mode laboratory and field measurements. *Atmos. Environ.* 132:1–10. doi:10.1016/j.atmosenv.2016.02.028.

Lee, R. F. 2008. *Phycology*. 4th ed. Cambridge, United Kingdom: Cambridge University Press. doi:10.1017/CBO9780511812897.

Lehahn, Y., I. Koren, Y. Rudich, K. D. Bidle, M. Trainic, J. M. Flores, S. Sharoni, and A. Vardi. 2014. Decoupling atmospheric and oceanic factors affecting aerosol loading over a cluster of mesoscale North Atlantic eddies. *Geophys. Res. Lett.* 41 (11):4075–81. doi:10.1002/2014GL059738.

Lei, Z., B. Chen, and S. D. Brooks. 2023. Effect of acidity on ice nucleation by inorganic–organic mixed droplets. *ACS Earth Space Chem.* 7 (12):2562–73. doi:10.1021/acsearthspacechem.3c00242.

Linge Johnsen, S. A., and J. Bollmann. 2020. Coccolith mass and morphology of different Emiliania huxleyi morphotypes: A critical examination using Canary Islands material. *PLoS One.* 15 (3):e0230569. doi:10.1371/journal.pone.0230569.

Manson, J. E. 1957. Calcium carbonate as an ice nucleus. *J. Meteorol.* 14 (1):85–6. doi:10.1175/0095-9634-14.1.85.

Matthews, B. H., A. N. Alsante, and S. D. Brooks. 2023. Pollen emissions of subpollen particles and ice nucleating particles. *ACS Earth Space Chem.* 7 (6):1207–18. doi:10.1021/acsearthspacechem.3c00014.

Matrai, P. A., and M. D. Keller. 1993. Dimethylsulfide in a large-scale coccolithophore bloom in the Gulf of Maine. *Cont. Shelf Res.* 13 (8-9):831–43. doi:10.1016/0278-4343(93)90012-M.

McCluskey, C. S., T. C. J. Hill, F. Malfatti, C. M. Sultana, C. Lee, M. V. Santander, C. M. Beall, K. A. Moore, G. C. Cornwell, D. B. Collins, et al. 2017. A Dynamic Link between Ice Nucleating Particles Released in Nascent Sea Spray Aerosol and Oceanic Biological Activity during Two Mesocosm Experiments. *J. Atmospheric Sci.* 74 (1):151–66. doi:10.1175/JAS-D-16-0087.s1.

Michaud, J. M., L. R. Thompson, D. Kaul, J. L. Espinoza, R. A. Richter, Z. Z. Xu, C. Lee, K. M. Pham, C. M. Beall, F. Malfatti, et al. 2018. Taxon-specific aerosolization of bacteria and viruses in an experimental ocean-atmosphere mesocosm. *Nat. Commun.* 9 (1):2017. doi:10.1038/s41467-018-04409-z.

Mitts, B. A., X. Wang, D. D. Lucero, C. M. Beall, G. B. Deane, P. J. DeMott, and K. A. Prather. 2021. Importance of Supermicron Ice Nucleating Particles in Nascent Sea Spray. *Geophys. Res. Lett.* 48 (3):e2020GL089633. doi:10.1029/2020GL089633.

Mojica, K. D. A., and C. P. D. Brussaard. 2014. Factors affecting virus dynamics and microbial host-virus interactions in marine environments. *FEMS Microbiol. Ecol.* 89 (3):495–515. doi:10.1111/1574-6941.12343.

Mukai, H., Y. Yokouchi, and M. Suzuki. 1995. Seasonal variation of methanesulfonic acid in the atmosphere over the oki islands in the sea of Japan. *Atmos. Environ.* 29 (14):1637–48. doi:10.1016/1352-2310(95)00057-6.

Murphy, D. M., and T. Koop. 2005. Review of the vapour pressures of ice and supercooled water for atmospheric applications. *Q J. R Meteorol. Soc.* 131 (608):1539–65. doi:10.1256/qj.04.94.

Murray, B. J., D. O'Sullivan, J. D. Atkinson, and M. E. Webb. 2012. Ice nucleation by particles immersed in supercooled cloud droplets. *Chem. Soc. Rev.* 41 (19):6519–54. doi:10.1039/c2cs35200a.

Nissimov, J. I., C. A. Worthy, P. Rooks, J. A. Napier, S. A. Kimmance, M. R. Henn, H. Ogata, and M. J. Allen. 2012. Draft Genome Sequence of the Coccolithovirus *Emiliania huxleyi* Virus 202. *J. Virol.* 86 (4):2380–1. doi:10.1128/jvi.06863-11.

Obata, T., S. Schoenefeld, I. Krahnert, S. Bergmann, A. Scheffel, and A. R. Fernie. 2013. Gas-chromatography mass-spectrometry (GC-MS) based metabolite profiling reveals mannitol as a major storage carbohydrate in the coccolithophorid Alga *Emiliania huxleyi*. *Metabolites.* 3 (1):168–84. doi:10.3390/metabo3010168.

Paasche, E. 2001. A review of the coccolithophorid *Emiliania huxleyi*. (prymnesiophyceae), with particular reference to growth, coccolith formation, and calcification-photosynthesis interactions. *Phycologia* 40 (6):503–29. doi:10.2216/i0031-8884-40-6-503.1.

Parsons, T. R., Y. Maita, and C. M. Lalli. 1984. *A manual of chemical and biological methods for seawater analysis*. Oxford, United Kingdom: Pergamon Press.

Patel, A., R. T. Noble, J. A. Steele, M. S. Schwalbach, I. Hewson, and J. A. Fuhrman. 2007. Virus and prokaryote enumeration from planktonic aquatic environments by epifluorescence microscopy with SYBR Green I. *Nat. Protoc.* 2 (2):269–76. doi:10.1038/nprot.2007.6.

Perkins, R. J., M. G. Vazquez de Vasquez, E. E. Beasley, T. C. J. Hill, E. A. Stone, H. C. Allen, and P. J. DeMott. 2020. Relating Structure and Ice Nucleation of Mixed Surfactant Systems Relevant to Sea Spray Aerosol. *J. Phys. Chem. A.* 124 (42):8806–21., 2020. doi:10.1021/acs.jpca.0c05849.

Polen, M., T. Brubaker, J. Somers, and R. C. Sullivan. 2018. Cleaning up our water: Reducing interferences from nonhomogeneous freezing of "pure" water in droplet freezing assays of ice-nucleating particles. *Atmos. Meas. Tech.* 11 (9):5315–34. doi:10.5194/amt-11-5315-2018.

Porter, G. C. E., M. P. Adams, I. M. Brooks, L. Ickes, L. Karlsson, C. Leck, M. E. Salter, J. Schmale, K. Siegel, S. N. F. Sikora, et al. 2022. Highly Active Ice-Nucleating Particles at the Summer North Pole. *J. Geophys. Res. Atmos.* 127 (6):e2021JD036059. doi:10.1029/2021JD036059.

Prather, K. A., T. H. Bertram, V. H. Grassian, G. B. Deane, M. D. Stokes, P. J. DeMott, L. I. Aluwihare, B. P. Palenik, F. Azam, J. H. Seinfeld, et al. 2013. Bringing the ocean into the laboratory to probe the chemical complexity of sea spray aerosol. *Proc. Natl. Acad. Sci. USA* 110 (19):7550–5. doi:10.1073/pnas.1300262110.

Pruppacher, H. R. and J. D. Klett. 1997. *Microphysics of clouds and precipitation*. 2nd ed. Dordrecht, the Netherlands: Kluwer Academic Publishers.

Quinn, P. K., and T. S. Bates. 2011. 7375. The case against climate regulation via oceanic phytoplankton sulphur emissions. *Nature*. 480 (7375):51–6. doi:10.1038/nature10580.

Rahlff, J., S. P. Esser, J. Plewka, M. E. Heinrichs, A. Soares, C. Scarchilli, P. Grigioni, H. Wex, H.-A. Giebel, and A. J. Probst. 2023. Marine viruses disperse bidirectionally along the natural water cycle. *Nat. Commun.* 14 (1): 6354.doi:10.1038/s41467-023-42125-5.

Rastelli, E., C. Corinaldesi, A. Dell'Anno, M. Lo Martire, S. Greco, M. Cristina Facchini, M. Rinaldi, C. O'Dowd, D. Ceburnis, and R. Danovaro. 2017. Transfer of labile organic matter and microbes from the ocean surface to the marine aerosol: An experimental approach. *Sci. Rep.* 7 (1):11475. doi:10.1038/s41598-017-10563-z.

Reicher, N., L. Segev, and Y. Rudich. 2018. The WeIzmann Supercooled Droplets Observation on a Microarray (WISDOM) and application for ambient dust. *Atmos. Meas. Tech.* 11 (1):233–48. doi:10.5194/amt-11-233-2018.

Rogers, D. C., P. J. DeMott, S. M. Kreidenweis, and Y. Chen. 1998. Measurements of ice nucleating aerosols during SUCCESS. *Geophys. Res. Lett.* 25 (9):1383–6. doi:10.1029/97GL03478.

Sanchez, K. J., C. L. Chen, L. M. Russell, R. Betha, J. Liu, D. J. Price, P. Massoli, L. D. Ziemba, E. C. Crosbie, R. H. Moore, et al. 2018. Substantial Seasonal Contribution of Observed Biogenic Sulfate Particles to Cloud Condensation Nuclei. *Sci. Rep.* 8 (1):3235. doi:10.1038/s41598-018-21590-9.

Schroeder, D. C., J. Oke, M. Hall, G. Malin, and W. H. Wilson. 2003. Virus succession observed during an Emiliania huxleyi bloom. *Appl. Environ. Microbiol.* 69 (5):2484–90. doi:10.1128/AEM.69.5.2484-2490.2003.

Schroeder, D. C., J. Oke, G. Malin, and W. H. Wilson. 2002. Coccolithovirus (Phycodnaviridae): Characterisation of a new large dsDNA algal virus that infects *Emiliana huxleyi*. *Arch. Virol.* 147 (9):1685–98. doi:10.1007/s00705-002-0841-3.

Sellegri, K., C. D. O'Dowd, Y. J. Yoon, S. G. Jennings, and G. de Leeuw. 2006. Surfactants and submicron sea spray generation. *J. Geophys. Res.* 111 (D22):58. doi:10.1029/2005JD006658.

Sharoni, S., M. Trainic, D. Schatz, Y. Lehahn, M. J. Flores, K. D. Bidle, S. Ben-Dor, Y. Rudich, I. Koren, and A. Vardi. 2015. Infection of phytoplankton by aerosolized marine viruses. *Proc. Natl. Acad. Sci. U S A* 112 (21): 6643–7. doi:10.1073/pnas.1423667112.

Shirai, Y., Y. Tomaru, Y. Takao, H. Suzuki, T. Nagumo, and K. Nagasaki. 2008. Isolation and characterization of a single-stranded RNA virus infecting the marine planktonic diatom *Chaetoceros tenuissimus meunier*. *Appl. Environ. Microbiol.* 74 (13):4022–7. doi:10.1128/AEM.00509-08.

Storelvmo, T., and I. Tan. 2015. The Wegener-Bergeron-Findeisen process - Its discovery and vital importance for weather and climate. Meteorologische Zeitschrift. 24 (4): 455–61. doi:10.1127/metz/2015/0626.

Suttle, C. A. 2007. Marine viruses - Major players in the global ecosystem. *Nat. Rev. Microbiol.* 5 (10):801–12. doi:10.1038/nrmicro1750.

Taylor, A. R., C. Brownlee, and G. Wheeler. 2017. Coccolithophore Cell Biology: Chalking Up Progress. *Ann. Rev. Mar. Sci.* 9 (1):283–310. doi:10.1146/annurev-marine-122414-034032.

Thornton, D. C., S. D. Brooks, E. K. Wilbourn, J. Mirrielees, A. N. Alsante, G. Gold-Bouchot, A. Whitesell, and K. McFadden. 2023. Production of ice-nucleating particles (INPs) by fast-growing phytoplankton. *Atmos. Chem. Phys.* 23 (19):12707–29. doi:10.5194/acp-23-12707-2023.

Trainic, M., I. Koren, S. Sharoni, M. Frada, L. Segev, Y. Rudich, and A. Vardi. 2018. Infection Dynamics of a Bloom-Forming Alga and Its Virus Determine Airborne Coccolith Emission from. *Seawater. iScience* 6:327–35. doi:10.1016/j.isci.2018.07.017.

Tsuji, Y., M. Yamazaki, I. Suzuki, and Y. Shiraiwa. 2015. Quantitative Analysis of Carbon Flow into Photosynthetic Products Functioning as Carbon Storage in the Marine Coccolithophore, *Emiliania huxleyi*. *Mar. Biotechnol.* 17 (4):428–40. doi:10.1007/s10126-015-9632-1.

Tyrrell, T., and A. Merico. 2004. *Emiliania huxleyi*: Bloom observations and the conditions that induce them. *Coccolithophores: From molecular processes to global impact*. Berlin, Heidelberg: Springer.

Vali, G. 1971. Quantitative evaluation of experimental results and the heterogeneous freezing nucleation of supercooled droplets. *J. Atmos. Sci.* 28 (3):402–9. doi:10.1175/1520-0469(1971)028<0402:QEOERA>2.0.CO;2.

Vardi, A., L. Haramaty, B. A. S. van Mooy, H. F. Fredricks, S. A. Kimmance, A. Larsen, and K. D. Bidle. 2012. Host-virus dynamics and subcellular controls of cell fate in a natural coccolithophore population. *Proc. Natl. Acad. Sci. USA* 109 (47):19327–32. doi:10.1073/pnas.1208895109.

Wilbourn, E. K., D. C. O. Thornton, C. Ott, J. Graff, P. K. Quinn, T. S. Bates, R. Betha, L. M. Russell, M. J. Behrenfeld, and S. D. Brooks. 2020. Ice Nucleation by Marine Aerosols Over the North Atlantic Ocean in Late Spring. *JGR. Atmospheres* 125 (4):e2019JD030913. doi:10.1029/2019JD030913.

Wilhelm, S. W., and C. A. Suttle. 1999. Viruses and Nutrient Cycles in the Sea. *Bioscience*. 49 (10):781–8. doi:10.2307/1313569.

Wilson, T. W., L. A. Ladino, P. A. Alpert, M. N. Breckels, I. M. Brooks, J. Browse, S. M. Burrows, K. S. Carslaw, J. A. Huffman, C. Judd, et al. 2015. A marine biogenic source of atmospheric ice-nucleating particles. *Nature*. 525 (7568):234–8. doi:10.1038/nature14986.

Wolf, M. J., A. Coe, L. A. Dove, M. A. Zawadowicz, K. Dooley, S. J. Biller, Y. Zhang, S. W. Chisholm, and D. J. Cziczo. 2019. Investigating the Heterogeneous Ice Nucleation of Sea Spray Aerosols Using *Prochlorococcus* as a Model Source of Marine Organic Matter. *Environ. Sci. Technol.* 53 (3):1139–49. doi:10.1021/acs.est.8b05150.

Yun, Y., and J. E. Penner. 2013. An evaluation of the potential radiative forcing and climatic impact of marine organic aerosols as heterogeneous ice nuclei. *Geophys. Res. Lett.* 40 (15):4121–6. doi:10.1002/grl.50794.

Zhao, X., X. Liu, S. M. Burrows, and Y. Shi. 2021. 2305. Effects of marine organic aerosols as sources of immersion-mode ice-nucleating particles on high-latitude mixed-phase clouds. *Atmos. Chem. Phys.* 21 (4):2327. doi:10.5194/acp-21-2305-2021.